AGU PUBLICATIONS

Tectonics

RESEARCH ARTICLE
10.1002/2015TC004044

Key Points:
- Thermochronology and stream profile analysis elucidate Cenozoic extension in the Southern Balkans
- The Strymon detachment did not lead to enhanced footwall erosion or basin development
- The West Pirin fault resulted in footwall erosion and formation of the Sandanski basin

Supporting Information:
- Supporting Information S1
- Table S2

Correspondence to:
K. Stübner,
konstanze.stuebner@uni-tuebingen.de

Citation:
Stübner, K., K. Drost, R. Schoenberg, M. Böhme, J. Starke, and T. A. Ehlers (2016), Asynchronous timing of extension and basin formation in the South Rhodope core complex, SW Bulgaria, and northern Greece, *Tectonics*, *35*, 136–159, doi:10.1002/2015TC004044.

Received 28 SEP 2015
Accepted 3 DEC 2015
Accepted article online 11 DEC 2015
Published online 19 JAN 2016

Asynchronous timing of extension and basin formation in the South Rhodope core complex, SW Bulgaria, and northern Greece

Konstanze Stübner[1], Kerstin Drost[1], Ronny Schoenberg[1], Madelaine Böhme[1,2], Jessica Starke[1], and Todd A. Ehlers[1]

[1]Department of Geosciences, University Tübingen, Tübingen, Germany, [2]Senckenberg Center for Human Evolution and Palaeoenvironment, Tübingen, Germany

Abstract Upper crustal extensional structures range from steep normal faults to shallow-dipping detachments. The relationship between extension and formation of synkinematic hanging wall basins including their relative timing is not well understood. The South Rhodope core complex, Southern Balkans, has experienced extension for >40 Ma leading to a number of extensional structures and Cenozoic sedimentary basins. We present new bedrock and basin detrital zircon and apatite (U-Th-Sm)/He ages from the Pirin and Rila Mountains and the Sandanski basin. Results identify three episodes of Cenozoic extension in SW Bulgaria accommodated by (1) the Eocene/Oligocene Mesta detachment; (2) the early to middle Miocene Gorno Spanchevo fault (circa 18–15 Ma), which is the northern prolongation of the Strymon low-angle detachment; and (3) the late Miocene West Pirin fault (≤10 Ma). Detachment faulting on the Strymon fault accommodated tens of kilometers of ENE-WSW extension and created ~1500 m topographic relief, but because the resulting hillslopes were gentle (≤10°), extension did not lead to enhanced footwall erosion or formation of a hanging wall basin. In contrast, the West Pirin normal fault resulted in mostly vertical motion of its footwall causing steep topography, rapid erosion, and formation of the synrift Sandanski basin. Digital topographic analysis of river channel profiles identifies the latest episodes of deformation including westward tilting of the Sandanski and Strymon basins and Quaternary N-S extension. This study demonstrates that basin formation in the South Rhodope core complex is related to normal faulting postdating the main episode of crustal stretching by detachment faulting.

1. Introduction

Following recognition that low-angle detachments facilitate exhumation of deeper crustal rocks [*Davis and Coney*, 1979; *Wernicke*, 1981; *Lister and Davis*, 1989], metamorphic core complexes have been documented in oceanic and continental settings worldwide including the extensional provinces of the Basin and Range (western U.S.) and the eastern Mediterranean [cf. *Whitney et al.*, 2013, and references therein]. Furthermore, low-angle detachments have also been identified in contractional tectonic settings such as the Alpine-Himalayan orogenic belt [e.g., *Ratschbacher et al.*, 1989; *Chen et al.*, 1990; *Stübner et al.*, 2013]. Many extensional structures are associated with sedimentary basins in their hanging wall [*Davis and Coney*, 1979; *Beratan*, 1996]. Basin development is generally coeval to extension both in normal fault and detachment systems [e.g., *Yarnold*, 1994; *Friedmann and Burbank*, 1995; *McClaughry and Gaylord*, 2005]. In some cases, multiphase basin evolution is documented with earlier supradetachment basins overprinted by later steep, brittle faults associated with their own sediment systems [*Coney and Harms*, 1984; *Bozkurt and Sözbilir*, 2004; *Oner and Dilek*, 2011]. In other examples, the kinematic relationship and relative timing of basin development and detachment faulting is disputed [e.g., *Ring et al.*, 2001]. However, many studies focus either on the structural-metamorphic(-magmatic) history of the exhumed basement gneiss or on the sedimentological evolution of the synextensional basin. Integrative studies are rare, and in many cases, the relationships between an extensional structure, exhumation of its footwall and basin development remain poorly understood. For example, *Oner and Dilek* [2011] emphasize a time gap of 0 to 13 Ma between the initiation of extension and the onset of syntectonic deposition in metamorphic core complexes worldwide. In the central Aegean Cyclades, unresolved relationships between detachment faulting and basin development lead to a dispute about the timing of initiation of lithospheric extension [cf. *Jolivet and Brun*, 2010; *Ring et al.*, 2010]. A discrepancy between the timing of extension and basin formation has been documented, in particular, in the Southern Balkans including the South Rhodope core complex (SRCC) [*Kounov et al.*, 2004;

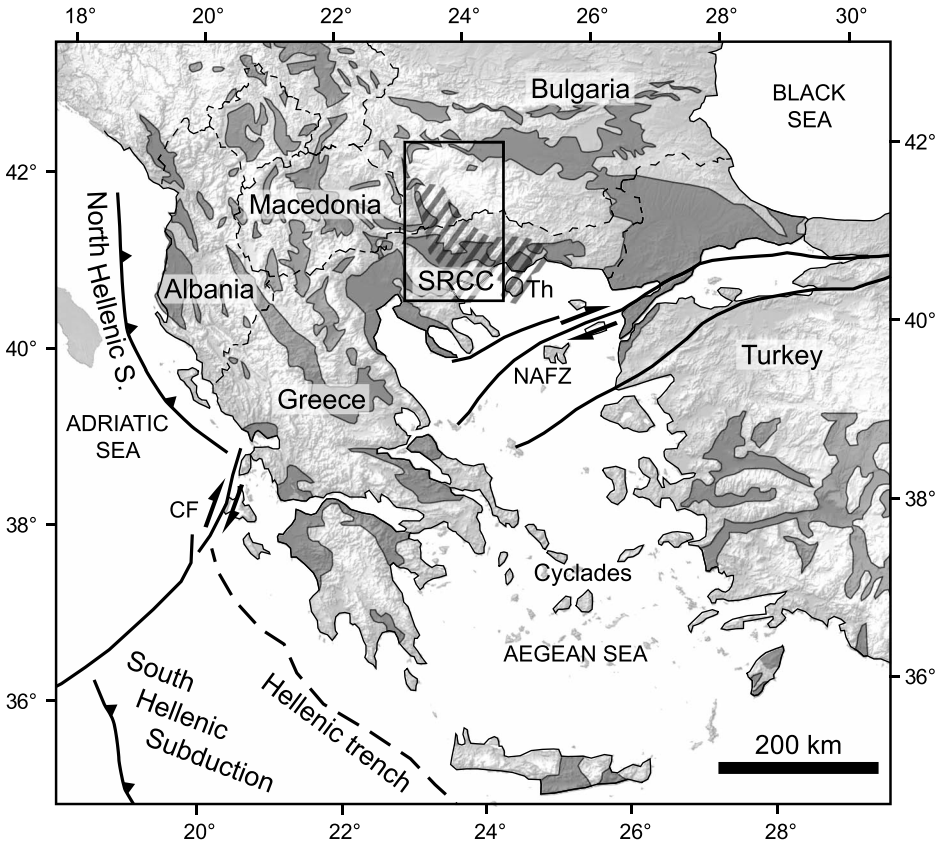

Figure 1. Overview map of the Aegean and southern Balkans. Main structures include the North and South Hellenic subduction zones, the North Anatolian fault zone (NAFZ), and Cephalonia transform fault (CF). Cenozoic sedimentary basins (dark grey) after *Burchfiel et al.* [2008] and *Hinsbergen et al.* [2010]. Hatched signature outlines the approximate extent of South Rhodope core complex (SRCC, *after Brun and Sokoutis* [2007]; Th, Thassos island). Rectangle indicates area of Figure 2. Modified from *Jolivet and Brun* [2010].

Brun and Sokoutis, 2007; *Burchfiel et al.*, 2008]. Integrated studies of extensional faults, footwall exhumation, and basin evolution are key to understanding extensional settings because the presence or absence of synextensional basins and the spatial and temporal relationship between basins and extensional structures (a) constrain the evolution of landscape and topographic relief [*Densmore et al.*, 2004, 2005] and (b) provide insight into the geodynamic cause and mode of extension (e.g., wide or narrow rift, core complex [*Friedmann and Burbank*, 1995; *Whitney et al.*, 2013]).

In the Southern Balkans (Figure 1) as much as 50 Ma of continuous or episodic Cenozoic extension resulted in Paleogene and Neogene basins with marine or continental sedimentary and volcanigenic deposits [*Krohe and Mposkos*, 2002; *Dumurdzanov et al.*, 2005; *Zagorchev*, 2007]. Basin-bounding structures comprise shallow-dipping detachments and steep normal faults of variable orientation. Extensional systems in the Southern Balkans and Aegean have been attributed to a variety of geodynamic causes including back-arc extension driven by Hellenic slab retreat, gravitational collapse of thickened continental crust, lithospheric stretching, mantle delamination, tearing of the subducting slab, and westward propagation of the North Anatolian fault [*Mercier et al.*, 1989; *Royden*, 1993; *Dinter and Royden*, 1993; *Armijo et al.*, 1999; *Brun and Sokoutis*, 2007; *Burchfiel et al.*, 2008; *Jolivet et al.*, 2010; *Royden and Papanikolaou*, 2011; *Kydonakis et al.*, 2015]. In northern Greece and SW Bulgaria (SRCC; Figure 1) geothermochronological, structural, and petrological data from basement exposure in combination with stratigraphic and structural data from Cenozoic basins yield a comprehensive albeit disputed picture of Cenozoic extension [*Dinter and Royden*, 1993; *Dinter*, 1998; *Wawrzenitz and Krohe*, 1998; *Brun and Sokoutis*, 2007; *Kounov et al.*, 2015]. In SW Bulgaria and Macedonia geochronological and thermochronological constraints on faulting and basement exhumation are scarce [*Burchfiel et al.*, 2003; *Kounov et al.*, 2004; *Georgiev et al.*, 2010], and the timing of

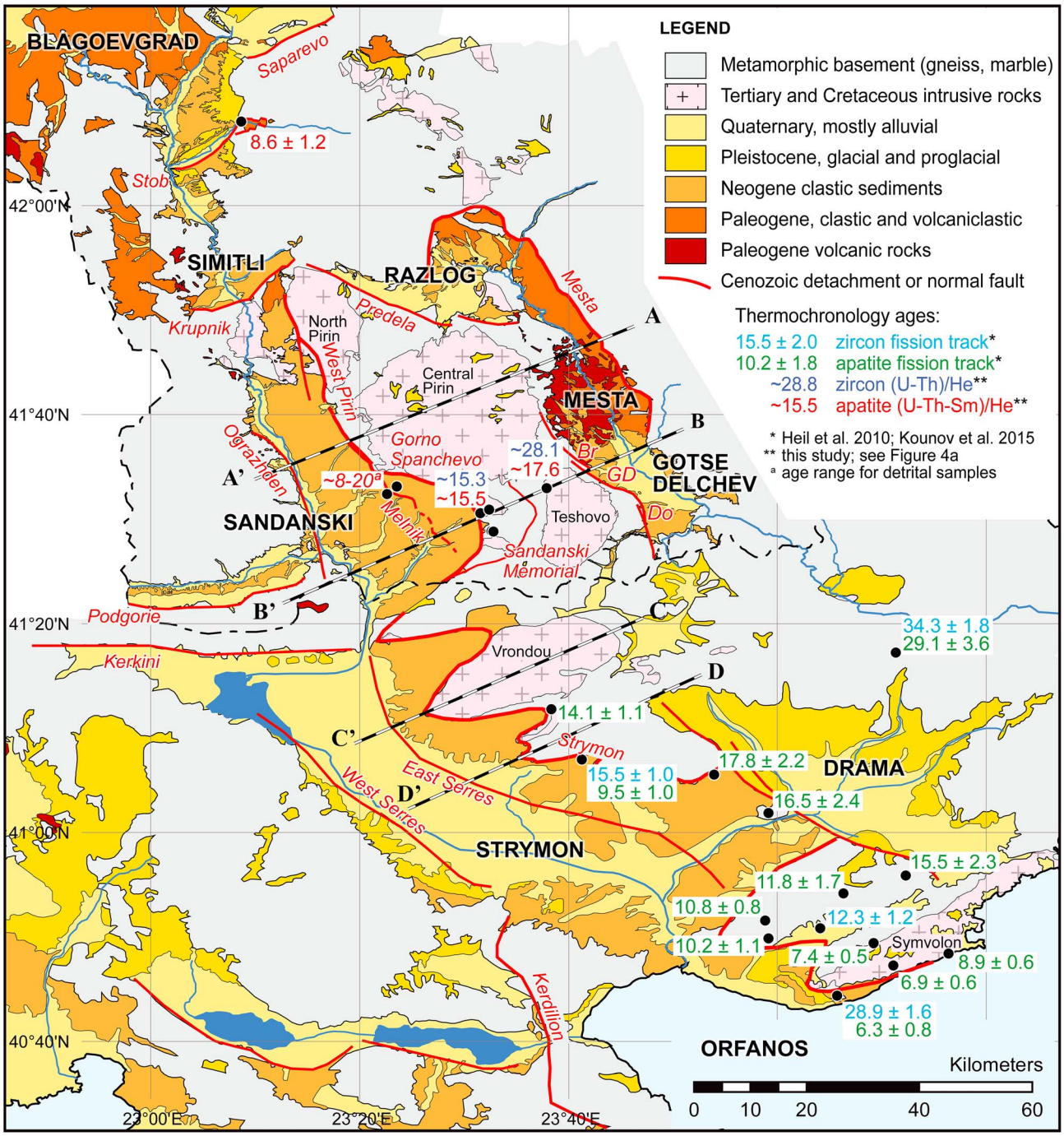

Figure 2. Simplified geologic map of SW Bulgaria and northern Greece compiled from 1:100.000 geologic maps of Bulgaria [*Zagorchev and Dinkova*, 1990] and 1:500.000 geologic map of Greece [*Bornovas and Rondogianni-Tsiambaou*, 1983] including adaptations from *Zagorchev* [1992], *Dinter* [1998], *Brun and Sokoutis* [2007], *Georgiev et al.* [2010], and own mapping. The map shows major Cenozoic basins (Blagoevgrad, Sandanski, Simitli, Razlog, Mesta, Gotse Delchev, Strymon, Drama, and Orfanos basins) and Cenozoic extensional structures (red lines and labels). Abbreviations are Br, Breznitsa fault; Do, Dobrotino fault; and GD, Gotse Delchev normal fault. See also Figure 5 for Cenozoic faults in SW Bulgaria. Thermochronology data are fission track ages from *Hejl et al.* [2010] and *Kounov et al.* [2015] in the Vrondou and Symvolon massifs of northern Greece and new (U-Th-Sm)/He data in SW Bulgaria. See Figure 4a for sample locations and age data from this study. Locations of profiles (Figures 7a–7d) are indicated.

Cenozoic extension is largely inferred from disputed biostratigraphic age constraints on basin sediments [*Dumurdzanov et al*., 2005; *Zagorchev*, 2007].

This study focuses on the Sandanski basin of SW Bulgaria [*Zagorchev*, 2007], a late Miocene half graben west of the Paleogene Mesta graben [*Burchfiel et al*., 2003] and north of the Eocene to Pliocene SRCC [*Dinter and Royden*, 1993; *Brun and Sokoutis*, 2007] (Figure 2). Aside from improving our understanding of extensional processes in the Southern Balkans, in general, we are motivated by the paleogeographic significance of this basin: Within Europe the Sandanski basin is a region with one of the most extensive occurrences of late Miocene mammal fossils, primarily found in 9–7 Ma fluvio-alluvial sediments in the southern part of the basin [e.g., *Spassov et al*., 2006]. During the late Miocene the Balkans have been part of the Greco-Iranian-Afghan faunal province [*De Bonis et al*., 1992] populated by the Pikermian Biome, which is characterized by very high diversity of open-country large mammals (e.g., cats, hyenas, horses, rhinos, antelopes, and giraffes) [*Bernor*, 1984; *Solounias et al*., 1999], including hominids [*Spassov et al*., 2012]. Many of the globally important Pikermian fossil localities are situated in SW Bulgarian basins [*Spassov*, 2002] adjacent to the Pirin, Rila, and Rhodope mountain ranges. However, the potential impacts of mountain building and development of a high-relief landscape on environmental change in the region and development of the Pikermian Biome have so far not been addressed, in part due to an incomplete understanding of the tectonic processes that led to the formation of these basins.

We present new apatite and zircon (U-Th)/He thermochronological data of bedrock samples from the Pirin Mountains in combination with detrital thermochronology of Sandanski basin sediments. We document three episodes of extension by low-angle detachment faulting in the early Oligocene and early to middle Miocene and by normal faulting on the West Pirin fault in the late Miocene. Although the earlier events likely created some topographic relief, only the late Miocene episode of extension led to the development of the Sandanski sediment basin and a high-relief mountain landscape. Furthermore, we present a geomorphic analysis of river profiles and channel steepness variations that documents the latest episodes of deformation including westward tilting of the Sandanski and Strymon basins and modern N-S extension reflected in the development of E-W striking Quaternary basins. The combination of thermochronologic and geomorphologic techniques offers a more complete picture of the evolution of the Southern Balkan extensional province. The presence or absence of synkinematic basins is attributed to the style of extension, i.e., steep normal faulting associated with rift flank uplift and footwall erosion and low-angle detachment faulting associated with gently dipping detachment surfaces, respectively. The different Cenozoic episodes of extension and their respective geomorphic and structural expressions reflect variable amounts of extension but are probably also affected by the rheological and thermal structure of the crust.

2. Geological Background

Regional extension since the early Cenozoic has shaped the Southern Balkans including Macedonia, southern Bulgaria, and northern Greece into a high-relief landscape controlled by fault-bounded basins and ranges [*Dumurdzanov et al*., 2005; *Kotzev et al*., 2006; *Zagorchev*, 2007] (Figure 1). The South Balkan extensional regime is linked with Cenozoic extension in the Aegean [*Dinter*, 1998; *Burchfiel et al*., 2000] and attributed to back-arc extension above the retreating Hellenic subduction zone [e.g., *Mercier et al*., 1989; *Royden*, 1993]. In the Aegean, Paleogene and Neogene extension is expressed in the Cycladic core complexes [*Gautier et al*., 1993; *Gautier and Brun*, 1994; *Jolivet and Brun*, 2010; *Jolivet et al*., 2010]. In the Southern Balkans, the best studied extensional system is the SRCC. It records $>$40 Ma of E-W to NE-SW extension accommodated by the middle Eocene to middle Oligocene Kerdilion and the Miocene Strymon detachments and represents the northern continuation of Aegean back-arc extension [*Dinter and Royden*, 1993; *Brun and Sokoutis*, 2007; *Kounov et al*., 2015] (Figure 2).

In the latest Miocene to early Pliocene westward propagation of the North Anatolian fault system decoupled the Aegean from the European hinterland, largely terminated stretching of the Aegean lithosphere and resulted in SW directed block motion of the Aegean relative to Europe [*McClusky et al*., 2000; *Papanikolaou and Royden*, 2007]. Latest Miocene to Pliocene E-W extension in the Southern Balkans—represented, for example, by the Strymon and Drama sedimentary basins—may be associated with dextral transtension along the North Anatolian fault [*Dinter and Royden*, 1993; *Dinter*, 1998] or continued west directed slab rollback along the North Hellenic trench [*Burchfiel et al*., 2008] (Figure 1). The switch to the modern N-S extensional

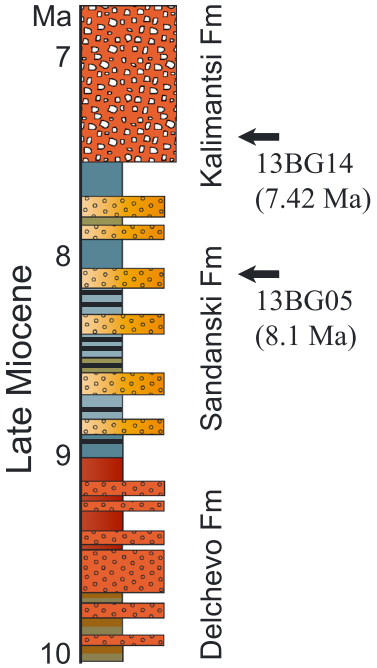

Figure 3. Simplified stratigraphic section of the Neogene Sandanski basin sediments based on *Zagorchev* [1992, 2007, and references therein] and own field mapping (M. Böhme et al., unpublished data, 2015). Age constraints are from unpublished paleomagnetic data (M. Böhme et al., unpublished data) and are broadly consistent with published biostratigraphic age constraints, although some authors have suggested older or younger ages for the beginning and end of deposition, respectively. Quaternary deposits (alluvial and periglacial clastics and fluvial river terraces along the Struma) are not shown. Arrows indicate positions of detrital thermochronologic samples and respective paleomagnetic ages (M. Böhme et al., unpublished data, 2015).

stress field is well documented in E-W trending Quaternary basins and seismically active or geomorphologically traceable faults [*Dumurdzanov et al*., 2005; *Burchfiel et al*., 2006; *Kotzev et al*., 2006], but its dynamic cause is poorly understood [*Burchfiel et al*., 2008].

2.1. Geology of the Sandanski Graben

The Sandanski basin in SW Bulgaria is a half graben bound in the east by the west dipping West Pirin and Gorno Spanchevo normal faults (Figure 2) [*Zagorchev*, 1992, 2007]. Subsidiary N-S striking normal faults occur within the basin (e.g., Melnik fault) and west of the graben (Ograzhden fault) [*Zagorchev*, 1992]. The stratigraphy of the Sandanski basin comprises proluvial to alluvial and fluvial-lacustrine sediments (fanglomerates, conglomerates, sandstones, siltstones, and lignites) of the Delchevo, Sandanski, and Kalimantsi Formations [*Kojumdgieva et al*., 1982] with a total thickness of ≥1500 m in the southern part of the basin.

The following overview of the Neogene stratigraphy is based on *Kojumdgieva et al*. [1982], *Zagorchev* [1992, 2007], *Klimov et al*. [2010, and references therein], and own field mapping (M. Böhme et al., unpublished data, 2015 Figure 3). The Delchevo Formation is a >200 m thick sequence of reddish and greenish, fluvial to alluvial bedded sandstones and conglomerates that is deposited unconformably on magmatic-metamorphic basement. Conformably above the Delchevo Formation, the Sandanski Formation consists of bluish, greenish, and yellowish alluvial to fluvial and lacustrine sandstones and conglomerates with interbeds of silt, clay, and coal. The Sandanski Formation is rich in mammal fossils of the Pikermian fauna [e.g., *Bernor*, 1984; *Spassov*, 2002; *Spassov et al*., 2006]. Its total thickness ranges from 200 m in the western part of the basin to probably 1000–1500 m in the south and east [*Kojumdgieva et al*., 1982; *Zagorchev*, 1992; *Klimov et al*., 2010]. The Kalimantsi Formation comprises reddish and yellowish coarse clastics including breccias, arcosic sandstones, and rare conglomerates. The component of granitic clasts in breccias increases upsection [e.g., *Zagorchev*, 1992, 2007]. The total thickness of the Kalimantsi Formation is 250–300 m [*Kojumdgieva et al*., 1982]. The formations are defined by their facies, and the deposits are diachronous with lateral transitions.

Depositional ages of the sequence are derived from biostratigraphic ages of fossiliferous beds, and there is general agreement that most of the sequence is late Miocene [e.g., *Zagorchev*, 2007, and references therein]. Sedimentation started at 9–10 Ma, a potential older onset of deposition [e.g., *Burchfiel et al*., 2000] is now refuted [e.g., *Spassov et al*., 2006]. Neogene deposition ended near the Miocene-Pliocene boundary based on scarce fossil evidence [*Spassov et al*., 2006]. Unpublished paleomagnetic age constraints (M. Böhme, unpublished data) support deposition of the Neogene sequence between ~10 and ~7 Ma (Figure 3).

The Neogene basin sediments are tilted ~5–20° to the east and interpreted as syntectonic strata. Opening of the Sandanski half graben has been related to the oldest sediments of the Delchevo Formation [*Zagorchev*, 2007] or the base of the Kalimantsi Formation [*Zagorchev*, 1992]. The West Pirin fault is a ~45–70° WSW dipping normal fault that offsets Neogene Sandanski basin sediments against strongly weathered basement rocks of the Pirin massif with a visible escarpment. Locally, for example, near the town of Ilindentsi, the fault

is capped by Pleistocene periglacial sediments [e.g., *Zagorchev*, 1992]. In the southern part of the basin, the steeply WSW dipping Melnik fault cuts the basin sediments forming an obvious fault scarp. Our mapping confirms the trace of the fault as shown in *Zagorchev* [1992] (Figure 2 and see also Figure 5). The footwall consists of Kalimantsi Formation; the hanging wall consists of a syntectonic megabreccia, approximately 500 m wide, with a lateral transition toward the basin into the Sandanski Formation (own observation). The Melnik fault is generally mapped as southward continuation of the West Pirin fault [*Zagorchev and Dinkova*, 1990; *Westaway*, 2006]; we discuss the two faults separately. A steeply dipping normal fault offsetting a megabreccia against Kalimantsi Formation in its footwall is also mapped in the northern part of the basin (*Zagorchev* [1992] and own observation).

South of the West Pirin fault, the boundary between Neogene sediments and basement of the southern Pirin massif is formed by the Gorno Spanchevo fault (GSF). Top-to-the-west to SW mylonites and ultramylonites in the metamorphic basement outline a shallowly ($\leq$30°) westward dipping ductile detachment overprinted by brittle deformation (cataclastic footwall rocks) [*Burchfiel et al*., 2000; *Georgiev et al*., 2010]. The detachment is eroded, and river channels incising into the basement are partly filled with Neogene sediments [e.g., *Zagorchev and Dinkova*, 1990; *Georgiev et al*., 2010]. *Georgiev et al*. [2010] report steeply dipping normal faults that overprint both the mylonitic basement and the Neogene sediments suggesting a long-lived tectonic evolution of this structure. At the southern end of the fault the contact between basement and Neogene sediments is capped by Pleistocene periglacial sediments [e.g., *Zagorchev*, 1992].

In the north, the Sandanski basin is terminated by the seismically active Krupnik normal fault and the Simitli basin [*Tranos et al*., 2006]. The Sandanski basin is aligned with Neogene-Quaternary Blagoevgrad basin in the north and the Strymon basin in northern Greece, which have been suggested to be kinematically related ("Struma lineament") [e.g., *Zagorchev*, 2007].

The highest mountains in SW Bulgaria including the Pirin (2914 m above sea level (asl)) and Rila (2925 m asl) massifs were glaciated during the Quaternary with maximum glaciation during the Last Glacial Maximum at 23–25 ka and 16–18 ka [*Kuhlemann et al*., 2013]. Equilibrium line altitudes were at ~2200 m asl; terminal moraines occur at elevations between 1800 and 2000 m asl on the southern and eastern sides of the massifs and as low as 1100–1400 m asl in some major glacial valleys on the northern and western sides [*Kuhlemann et al*., 2013].

3. Approach and Methods

We use low-temperature thermochronology (zircon and apatite (U-Th-Sm)/He dating; ZHe; AHe) of bedrock samples from the Pirin Mountains to obtain radiometric age constraints on their exhumation history. In addition, we obtained AHe ages from the Rila massif adjacent to the Blagoevgrad basin and from sedimentary samples from the Sandanski basin (Figure 2).

Thermochronologic data assess rock cooling histories on relatively long timescales of several million years and longer. On shorter ($<$1 Ma) timescales, the geomorphic response of drainage basins to climate and deformation history is imprinted in the longitudinal river profiles, incision rates, and channel gradients [*Kirby and Whipple*, 2001; *Duvall et al*., 2004; *Finnegan et al*., 2005; *Whittaker et al*., 2007]. Short-term changes such as normal faulting produce knickzones and variations in drainage basin slope-area relationships [*Whipple and Tucker*, 1999; *Reinhardt et al*., 2007; *Boulton and Whittaker*, 2009; *Loget and van den Driessche*, 2009]. We compliment our longer-timescale analysis from thermochronology with river profile analysis based on the analysis of a 30 m resolution digital elevation model (Aster) of SW Bulgaria to scrutinize landscape morphology on a regional scale and identify potential areas of recent or active faulting and tectonic uplift.

3.1. (U-Th-Sm)/He Thermochronology

The apatite and zircon (U-Th-Sm)/He (AHe, ZHe) dating was conducted at the thermochronology lab at the University of Tübingen. Clear apatite grains without inclusions or any other impurities or cracks were handpicked using a binocular microscope equipped with transmitted and reflected light and a polarizer and analyzer at 160X magnification. Zircon grains were selected based on grain shape and size. Alpha-ejection correction factors were calculated from measured grain dimensions after *Farley* [2002] and *Hourigan et al*. [2005] for apatite and zircon, respectively. Helium was measured on a Patterson helium extraction line. Concentrations of U, Th, and Sm were determined by isotope dilution inductively coupled plasma–mass

spectrometry (ID-ICP-MS). The apatite and zircon dissolution protocol and setup of the ICP-MS for (U-Th-Sm)/He dating at the University of Tübingen were developed in the course of this study, and we provide a detailed method description in the supporting information. The analytical uncertainty of ICP measurements is reported as 2 standard deviations (%). For helium measurements the analytical uncertainty is $<$2% and not reported. Because the reproducibility of single-grain aliquots constitutes a much larger uncertainty compared to analytical uncertainties, we report the unweighted mean (U-Th-Sm)/He age and 1 standard deviation (SD) as the uncertainty on the sample age. We interpret thermochronometer ages using closure temperatures of 180°C for ZHe [*Reiners et al.*, 2004] and 75°C for AHe [*Farley*, 2002].

3.2. River Profile Analysis

The normalized channel steepness index (ks_n) [*Wobus et al.*, 2006] was calculated to characterize the geometry of river longitudinal profiles. The stream power law [*Sklar and Dietrich*, 1998; *Whipple and Tucker*, 1999] shows the relationship between slope and drainage area as $S = ks\, A - \theta$, where S is the channel slope, ks is the steepness index, A is the upstream drainage area, and θ is the concavity [*Flint*, 1974; *Kirby and Whipple*, 2001; *Wobus et al.*, 2006]. We calculated the normalized ks (ks_n) by using a reference concavity of $\theta = 0.45$. The advantage in using ks_n is to detect the difference between the channel steepness of each segment of the river and the steepness of an equilibrium river [*Ouimet et al.*, 2009; *Whittaker*, 2012], which facilitates the comparison between different geographic regions [*Safran et al.*, 2005; *Cyr et al.*, 2010]. To extract the slope-area relationship, we used a 30 m resolution Aster digital elevation model (DEM), a smoothing window of 500 m and a contour sampling interval of 20 m. The calculation was performed using the ArcGIS stream profiler toolbox and MATLAB programs of *Whipple et al.* [2007].

4. Results

4.1. Thermochronology

We obtained apatite (U-Th-Sm)/He (AHe) ages from five granitic bedrock samples from a transect across the southern Pirin from the GSF (622 m asl) to the drainage divide between Struma and Mesta (1411 m asl; 13BG06 to 13BG12; Table 1 and Figure 4a; see Table S2 in the supporting information for complete data set). Single-grain ages range from 0.1 to 30.6 Ma, but most ages are between 13.5 and 19.4 Ma. One sample from the Rila (13BG01) yielded 6.8 to 9.4 Ma and one older age (23.6 Ma). Excluding single-grain ages that deviate by $>$20% from the sample mean ages are 8.6 ± 1.2 Ma (uncertainties are reported as 1 SD) for 13BG01 (Rila) and 15.2 ± 1.5 to 17.6 ± 2.0 Ma for the southern Pirin (Table 1 and Figure 4a). Sample 13BG06 yielded low He signals generally less than twice the blank level and accordingly a large variation in single-grain ages (0.1 to 28.7 Ma). No sample mean was calculated, and the sample is excluded from the interpretation. Although the AHe sample mean ages from the southern Pirin are indistinguishable within error, the mean ages increase with elevation and with distance to the GSF (Figures 4b and 4c). Sample 13BG01 is from a low elevation (548 m asl) $<$1 km away from the Stob fault that separates the Rila from the Blagoevgrad basin. The sample is $>$6 Ma younger than southern Pirin samples from a similar structural and topographic position; higher-elevation samples collected from the Rila did not yield apatite in sufficient quantity and quality to obtain AHe data.

Three samples from the southern Pirin resulted in zircon (U-Th)/He (ZHe) ages. ZHe single-grain ages reproduce well; the mean age of 13BG12 is significantly older than the corresponding AHe age (ZHe: 28.1 ± 1.6 Ma; AHe: 17.6 ± 2.0 Ma); for 13BG08 and 13BG09 the ZHe ages are within 1 SD identical to their AHe age (13BG08 ZHe: 15.2 ± 1.6 Ma, AHe: 15.2 ± 1.5 Ma; 13BG09 ZHe: 15.5 ± 0.9 Ma; AHe: 17.3 ± 1.2 Ma; Table 1 and Figures 4a–4c).

Two samples from the Neogene sediments were analyzed for detrital AHe ages (Table 2 and Figure 4d; see Table S2 in the supporting information for complete data set). 13BG05 is from the upper Sandanski Formation. Paleomagnetic data suggest a deposition age of 8.1 Ma (M. Böhme, unpublished data). 13BG14 is from the Kalimantsi Formation and has a paleomagenetic age of 7.42 Ma (M. Böhme, unpublished data). Both samples are from sand lenses within fluvial conglomerate and coarse sand deposits. Detrital AHe ages range from 8.7 to 42.6 Ma (13BG14) and 7.0 to 36.2 Ma (13BG05). Almost all detrital AHe ages are older than the depositional age of the samples consistent with the paleomagnetic and biostratigraphic ages of the formations. Taking into account the reproducibility of bedrock AHe ages (SD 0.5 to 2.0 Ma) the youngest grain of sample 13BG05 (7.0 Ma) is within the uncertainty of the method identical to the depositional age. In both samples 10% of the grains are less than 2 Ma older than the depositional age, 50% are less than 5 Ma older.

Table 1. Sample Locations and Summary of Bedrock (U-Th-Sm)/He Results

Sample	Latitude (°N)	Longitude (°E)	Elevation (m asl)	Distance to Gorno Spanchevo Fault (km)	Ft-corrected Age (Ma)	Average Age (Ma)	1 SD (Ma)
				Bedrock Zircon (U-Th)/He			
13BG08	41.50834	23.52603	622	0.5	14.0	15.2	1.6
					14.5		
					16.9		
13BG09	41.51396	23.53985	745	1.8	16.0	15.5	0.9
					15.8		
					14.1		
					16.1		
13BG12	41.54835	23.63218	1411	10.5	29.8	28.1	1.6
					26.5		
					28.1		
				Bedrock Apatite (U-Th-Sm)/He			
13BG01	42.13172	23.14420	548		8.9	8.6	1.2
					23.6[a]		
					6.8		
					9.4		
					9.2		
13BG06	41.47964	23.54633	702	1.6	7.6	no average calculated	
					28.7		
					0.1		
					10.3		
					8.3		
13BG07	41.47990	23.54378	675	1.4	15.3	15.7	0.5
					21.5[a]		
					16.1		
13BG08	41.50834	23.52603	622	0.5	16.1	15.2	1.5
					13.5		
					16.1		
13BG09	41.51396	23.53985	745	1.8	17.4	17.3	1.2
					18.4		
					16.0		
					30.6[a]		
13BG12	41.54835	23.63218	1411	10.5	17.2	17.6	2.0
					19.4		
					18.7		
					15.0		

[a]Outlier because of low ^{4}He signal close to blank level, or because age deviates >20% from sample average.

The age distributions are relatively narrow and almost identical for both samples with median ages of 13.1 Ma (13BG14) and 14.9 Ma (13BG05; Table 2). Figure 4d shows single-grain ages and kernel smoothing functions for both detrital samples (green and blue) and for all bedrock ages from the Pirin (red). Both the kernel smoothing functions of all bedrock ages (dashed red) and the outlier-corrected bedrock data set (solid red) have a narrow peak at ~16.5 Ma, i.e., older than >80% of the detrital ages from both samples. Mean ages ± 1 SD for the data sets are 16.6 ± 1.7 Ma for the outlier-corrected bedrock data and 13.2 ± 2.9 Ma (13BG14) and 14.0 ± 2.8 Ma (13BG05) for the detrital samples excluding four data points >25 Ma (Figure 4d). Figure 4e combines our new (U-Th-Sm)/He data with published apatite and zircon fission track ages from the footwall of the Strymon detachment in the southern SRCC (Figure 2) [*Hejl et al*., 2010; *Kounov et al*., 2015].

4.2. River Profile Analysis

Equilibrated rivers that flow through uniform lithology are expected to show constant channel steepness and a simple concave-up form along the course of the river. Variations in channel steepness may result, for example, from lithological variations, i.e., erodibility of the channel bed, or variable tectonic uplift rates, i.e., offset in uplift rates across a fault, regional tilting, or a change in uplift rate or base level within the time frame of geomorphic response [*Whipple and Tucker*, 1999; *Lavé and Avouac*, 2001; *Whipple*, 2004; *VanLaningham et al*., 2006;

Korupand Montgomery, 2008]. These processes result in a break of slope in the slope-area scaling and are expressed as knickzones and knickpoints along the course of a river and are consequently displayed in the variations of the channel steepness [*Whipple and Tucker*, 1999; *Reinhardt et al.*, 2007; *Loget and van den Driessche*, 2009].

Figure 5 illustrates the mean channel steepness index as averaged ks_n values from SW Bulgaria and the northern Strymon basin on a shaded relief map. The range of calculated ks_n values is similar throughout the study area (0 to 720). Low steepness ($ks_n \leq 25$) is generally found not only in Quaternary basins (Figure 5; Strymon, Razlog, Gotse Delchev basins) but also in the Neogene deposits of the southern Sandanski and Blagoevgrad

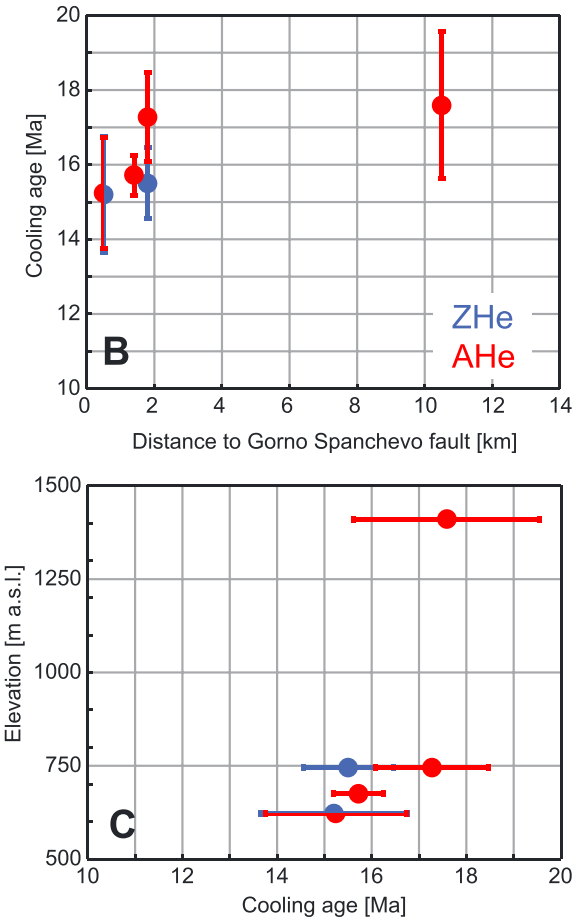

Figure 4. Overview of (U-Th-Sm)/He thermochronology data of the Rila and Pirin Mountains and Sandanski basin. (a) Sample locations, names, and ZHe (blue) and AHe (red) ages ±1 SD shown on an Aster DEM shaded relief. Locations and names of detrital samples are in italic letters. Main faults and basin stratigraphy as in Figures 2 and 5. (b) AHe and ZHe cooling ages versus distance to the Gorno Spanchevo fault. AHe and ZHe ages of sample 13BG08 overlap and are therefore shown as half circles. (c) AHe and ZHe cooling ages versus elevation. The trace of the Gorno Spanchevo fault is at an elevation of 600 to 700 m asl. (d) Age distributions of Pirin bedrock and Sandanski basin detrital samples. Lines are kernel smoothing functions for all bedrock AHe ages (dashed red) and bedrock AHe ages corrected for outliers (see section 4.1 for outliers; solid red). Single-grain ages are shown as red circles (outliers) and solid dots at arbitrary *y* value. Detrital samples are shown in green (13BG14) and blue (13BG05). Vertical lines represent depositional age (paleomagnetic data from M. Böhme (unpublished data)) of detrital samples. Mean ages ±1 SD are given for outlier-corrected bedrock data and for all detrital ages <25 Ma. (e) Cooling age versus elevation for our new AHe data from the southern Pirin (red) and apatite fission track ages from the northern Strymon (Vrondou massif, green) and southern Strymon basement (Symvolon massif, blue; see Figure 2) [*Hejl et al.*, 2010; *Kounov et al.*, 2015]. Zircon (U-Th)/He and fission track ages are also shown as diamonds with black outline. Thick colored lines illustrate the age-elevation trends for the three data sets; the trend for the Vrondou massif is poorly constrained, but on average, AFT ages are older than AFT ages from the Symvolon massif, and slightly younger than AHe ages from the Pirin massif; i.e., the timing of cooling increases from south to north.

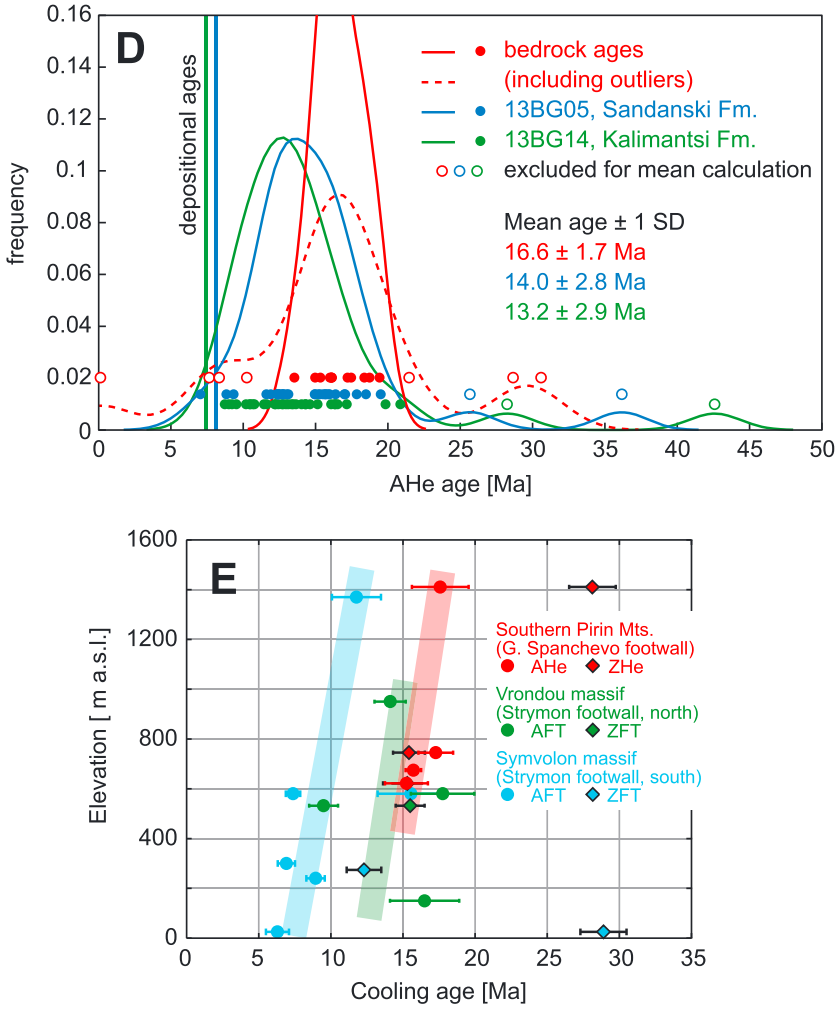

Figure 4. (continued)

basins. The steepest river sections are recorded in the Kresna gorge at the northern end of the Sandanski graben ($ks_n > 500$) and in a few glacially shaped tributaries of the Struma River, which drain the Rila, Pirin, and Ograzhden massifs.

The boundary between Cenozoic basins and basement typically corresponds to an increase in channel steepness index with ks_n values of 150–250 within 5 km upstream of the lithologic boundary. This change may be attributed to the variable erodibility of basement (mostly granitic and gneissic) and unsolidified Cenozoic sediments. However, the same lithologic boundary is not everywhere associated with a change in channel steepness (e.g., eastern and southern margins of the gneissic Ograzhden Mountains, southern

Table 2. Age Statistics of Detrital Thermochronology Samples

Sample	13BG14	13BG05
Latitude	41.55537°N	41.54311°N
Longitude	23.38318°E	23.36884°E
Elevation	555 m asl	420 m asl
Stratigraphic position	Kalimantsi Formation	Sandanski Formation
Paleomagnetic age of deposition:	7.42 Ma	8.1 Ma
Minimum AHe age	8.7 Ma	7.0 Ma
Maximum AHe age	42.6 Ma	36.2 Ma
Median	13.1 Ma	14.9 Ma
Mean age ±1 SD (excluding two old grains)	13.2 ± 2.9 Ma	14.0 ± 2.8 Ma

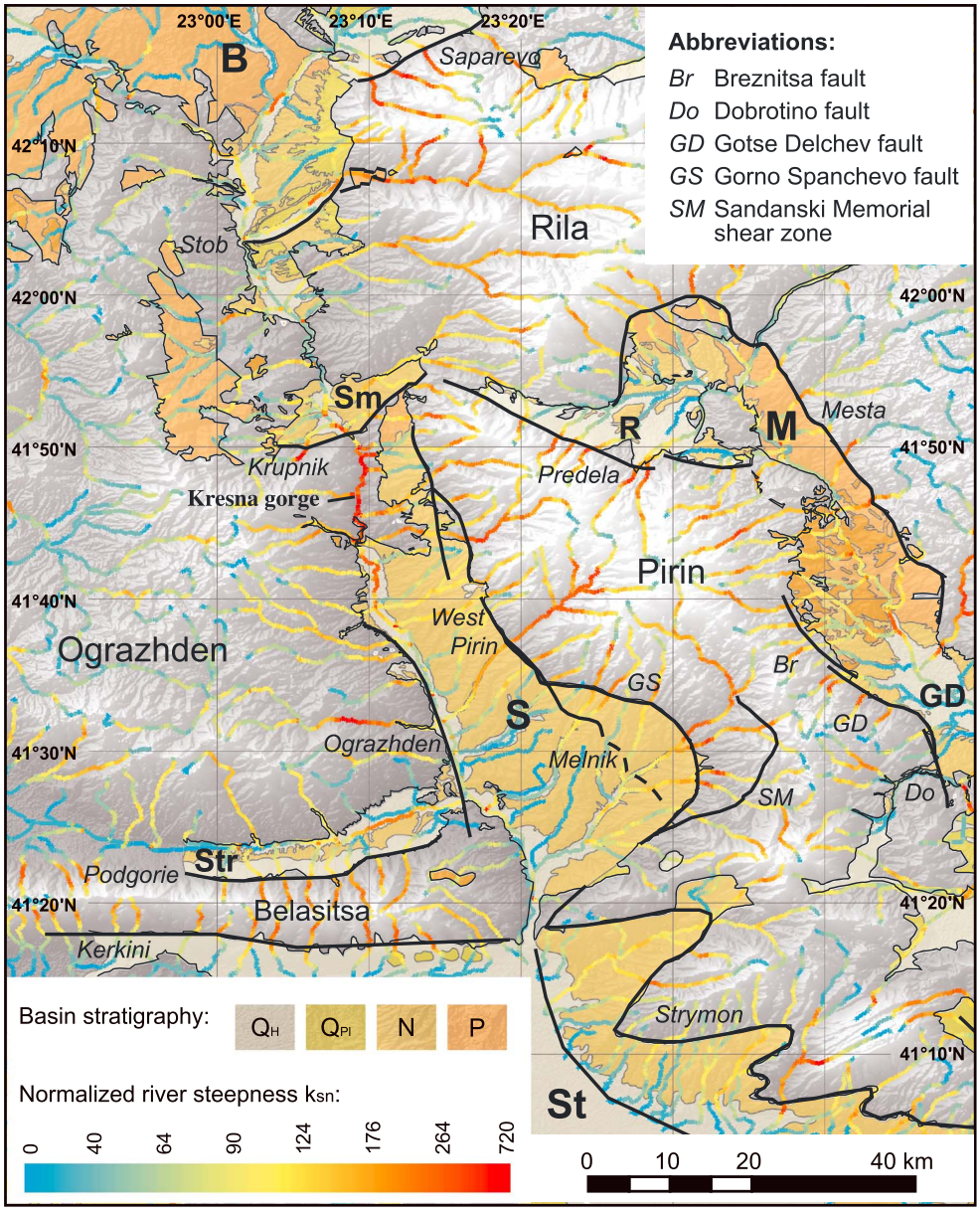

Figure 5. Overview of geomorphologic analysis of the study area. River steepness indices are shown as ks_n values on a shaded relief Aster digital elevation model; color scheme is ESRI ArcGIS Natural breaks (Jenks). Shaded areas show Cenozoic sedimentary and volcanic deposits (Q_H, Holocene, mostly alluvial; Q_{Pl}, Pleistocene; N, Neogene; P, Paleogene, clastic, and volcanigenic). Basins are B, Blagoevgrad; GD, Gotse Delchev; M, Mesta; R, Razlog; S, Sandanski; Sm, Simitli; St, Strymon; and Str, Strumitsa. Black lines are Cenozoic faults and shear zones [after *Zagorchev*, 1992; *Meyer et al.*, 2002; *Burchfiel et al.*, 2003; *Tranos et al.*, 2006; *Westaway*, 2006; *Zagorchev*, 2007; *Georgiev et al.*, 2010] labeled in italic letters.

margin of the Vrondou pluton, and western margin of Blagoevgrad basin; Figure 5) suggesting that at least in some cases the channel steepness index may indicate active or young (≤1 Ma) faulting and tectonic uplift of the basement such that a knickpoint migrating upstream causes a local high in the observed ks_n values.

We paid special attention to streams that flow from the Pirin and Ograzhden massifs into the Sandanski basin to test for potential recent activity on the basin-bounding faults. In addition to the regional distribution of ks_n values (Figure 5), we calculated longitudinal river profiles of streams from the Pirin massif (Figure 6; see Figure S1 in the supporting information for locations). Knickpoints were detected in most of the rivers within the granitic-gneissic basement 2–5 km upstream of the trace of the GSF and West Pirin fault and

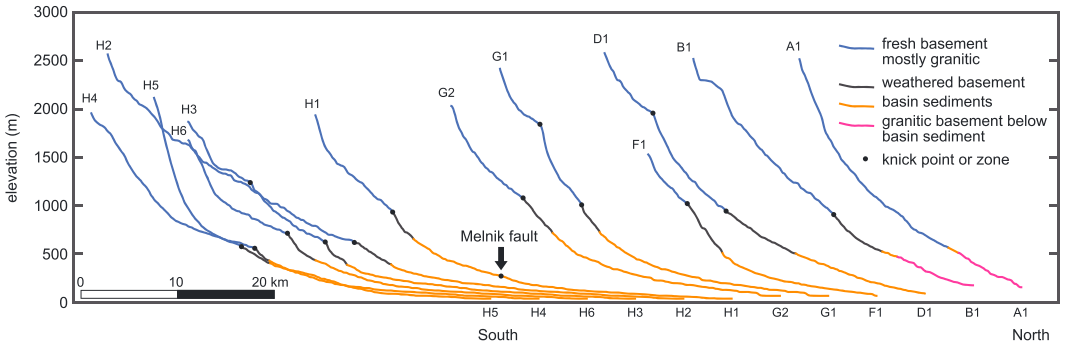

Figure 6. River profiles of the main tributaries from the Pirin Mountains into the Struma River (Strahler order 5 and 6), color coded by lithology of the channel bed. Streams from north (A1) to south (H5) are aligned by their confluence with the Struma River with a 5 km horizontal offset. See supporting information Figure S1 for stream locations. Knickpoints or knickzones detected in slope-drainage area relationships and longitudinal river profiles are indicated by black points. Knickpoints 200–500 m above the surface of basin sediments are attributed to a lithological contrast between fresh and weathered basement rocks. Higher-elevation knickpoints in streams H3, G1, and D1 are related to Pleistocene glaciation. In stream H1, a knickpoint within the basin occurs at the intersection with the Melnik fault.

200–400 m above the surface of the sediments (Figure 6). In stream H1 there is an additional knickpoint at its intersection with the Melnik fault (Figure 6; see also Figure S1). Knickpoints were also detected farther upstream at elevations between ~1200 m asl (stream H3) and ~1900 m asl (streams G1 and D1; Figure 6).

Tributaries from the Ograzhden massif west of the basin are smaller than those from the Pirin massif. Their steepness and concavity values are generally similar. Because the streams from the Ograzhden massif intersect the Ograzhden fault close to their confluence with the Struma River, river profile analysis did not reveal conclusive evidence for or against recent fault activity.

5. Discussion

5.1. Mesta Detachment: Oligocene Exhumation

The Teshovo pluton in the southern Pirin was emplaced in the early Oligocene (crystallization age 32 ± 0.2 Ma) [*Jahn-Awe et al.*, 2010] and cooled rapidly below closure of the ZHe system (13BG12: 28.1 ± 1.6 Ma). Assuming a crystallization temperature of ~700°C, the cooling rate is on the order of 130–260°C/Ma and consistent with rapid tectonic exhumation following its emplacement in an extensional environment [*Georgiev et al.*, 2010]. East of the Pirin the westward dipping Mesta detachment accommodated ENE-WSW extension from the late Eocene until the Oligocene [*Georgiev et al.*, 2010] or the early Miocene [*Burchfiel et al.*, 2003]. *Burchfiel et al.* [2003] propose that the Pirin forms the hanging wall of the Mesta detachment. In contrast, our Oligocene ZHe cooling ages suggest that the Pirin is part of the Mesta detachment footwall exhumed rapidly during extension. This interpretation is consistent with the model of *Georgiev et al.* [2010] and *Jahn-Awe et al.* [2010] who suggest that the Mesta detachment forms an anticline above the current exposure of the Pirin [*Jahn-Awe et al.*, 2010, Figure 5] (see also Figure 7b). The folded detachment is exposed in the eastern Pirin (early top-up-to-the-west shear on the Breznitsa and Dobrotino shear zones), and in the mylonitic to cataclastic Sandanski Memorial shear zone on the western side of the Pirin [*Georgiev et al.*, 2010; *Jahn-Awe et al.*, 2010] (see Figure 2 for fault locations). Although the Mesta detachment is considered inactive by 32 Ma (ductile fabric of Breznitsa and Dobrotino shear zones is cut by Central Pirin pluton) [*Georgiev et al.*, 2010], continued exhumation in the late Oligocene was facilitated by cataclastic normal faults on both sides of the Pirin massif (Sandanski Memorial shear zone and Breznitsa and Dobrotino faults) [*Georgiev et al.*, 2010; *Jahn-Awe et al.*, 2010].

5.2. Gorno Spanchevo Fault: Early to Middle Miocene Exhumation

The AHe age of 13BG12 and ZHe and AHe ages of the western Pirin samples (13BG07–13BG09) record rapid early to middle Miocene (17.6 ± 2.0 to 15.2 ± 1.5 Ma) cooling through the ZHe and AHe closure temperatures (Figures 4b and 4c). All ages are indistinguishable at the 1 SD level precluding meaningful calculation of a cooling rate. Nevertheless, the limited range in cooling ages (~2 Ma) indicates cooling of the western Pirin at >50°C/Ma. The nearly invariant age-elevation relationship of AHe samples (Figure 4c) further corroborates rapid exhumation and cooling in the early to middle Miocene. Near the trace of the GSF the amount of

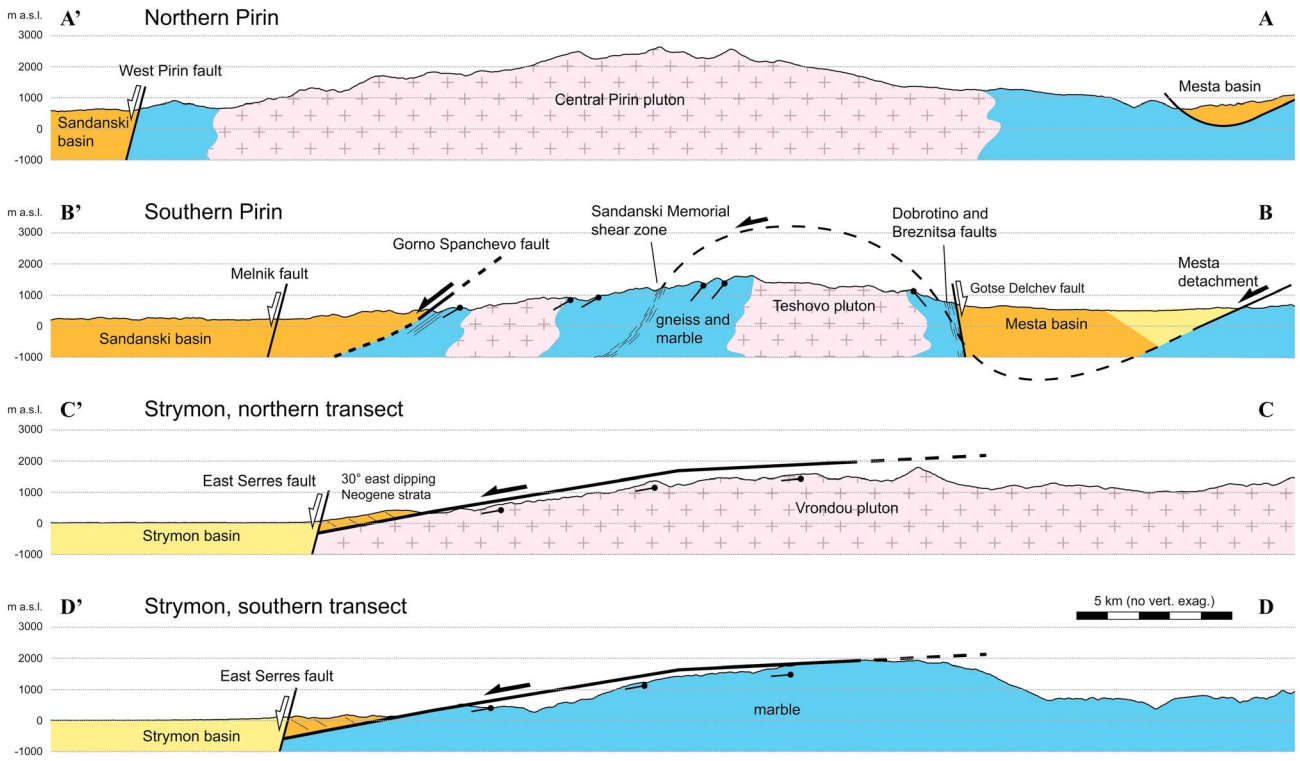

Figure 7. NE-SW profiles across (a) the northern Pirin, (b) the Gorno Spanchevo fault and southern Pirin, and (c, d) the Strymon detachment and Strymon basement in northern Greece (Vrondou pluton and marble exposure south of the pluton). Legend as in Figure 2. Tadpoles indicate schematically dip of foliation; structural data from *Jahn-Awe et al*. [2010] (profile in Figure 7b) and *Dinter* [1998] (profiles Figures 7c and 7d). Black arrows are Paleogene to early Miocene detachment faults; white arrows are late Miocene to Quaternary normal faults. In Figure 7b the geometry of the folded Mesta detachment is after *Jahn-Awe et al*. [2010]. The Sandanski Memorial shear zone and Breznitsa and Dobrotino faults are late Eocene and late Oligocene brittle-ductile to brittle faults, respectively, exhuming the Teshovo pluton in the footwall of the Mesta detachment. In contrast to the transects farther south, the surface of the Gorno Spanchevo-Strymon detachment is eroded and could not be reconstructed. The transect across the northern Pirin (Figure 7a) reveals a greater width of the massif compared to the southern Pirin and higher topography with peak elevations >2500 m asl. We suggest that this difference results from late Miocene uplift accommodated by the West Pirin normal fault, which exhumed deeper levels of the Pirin massif compared to those farther south. The early to middle Miocene Gorno Spanchevo-Strymon detachment either did not continue northward beyond the southern Pirin or was uplifted subsequently and eroded.

exhumation was sufficient to expose rocks from below the ZHe closure isotherm. For example, for a thermal gradient of 30°C/km rocks from ≥6 km depth are exposed. This depth estimate is consistent with textures of the exhumed shear zone (e.g., recrystallized quartz veins indicating ≥300°C) [*Georgiev et al*., 2010]. Near the crest between the Mesta and Sandanski basin, the unreset 28.1 ± 1.6 Ma ZHe age of 13BG12 limits the amount of Miocene exhumation to <6 km. The pattern of ZHe ages and the increase of AHe ages with distance to the GSF (Figure 4b) suggest that early to middle Miocene cooling is controlled by the GSF.

Apatite fission track ages (AFT) from the footwall of the Strymon detachment (Figure 2) [*Hejl et al*., 2010; *Kounov et al*., 2015] are also early to middle Miocene and range from 6.9 ± 0.6 Ma in the south to 14.1 ± 1.1 Ma in the north. Zircon fission track ages (ZFT) are only slightly older (12.3 ± 1.2 and 15.5 ± 1.0 Ma; Figure 2). Older ages are recorded in the hanging wall of the Strymon detachment (ZFT 28.9 ± 1.6 Ma) and east of the Drama basin (Oligocene AFT and ZFT ages). The distance of the samples to the fault trace varies and is difficult to estimate because of the corrugated geometry of the Strymon detachment (mullion structures after *Dinter and Royden* [1993]; Figure 2). In general, the AFT ages increase from SW to NE parallel to the transport direction of the Strymon detachment [*Dinter*, 1998]. AFT age-elevation relationships (Figure 4e) reveal a consistent first-order pattern: (1) for each region (south Pirin, Vrondou, and Symvolon) cooling ages increase only slightly with elevation suggesting rapid cooling, and (2) taking into account the different closure temperatures (AFT 110°C; AHe 75°C), the time of cooling becomes younger from the north toward the south (Figure 4e).

Based on the (U-Th)/He and fission track cooling ages we suggest that (1) rapid Miocene exhumation and cooling of the Pirin, Vrondou, and Symvolon massifs was accommodated by the GSF and the Strymon

detachment, which are segments of one continuous detachment fault, and (2) the latest stages of tectonic exhumation were diachronous from early to middle Miocene in the north to middle to late Miocene in the south.

5.3. Geometry of the Gorno Spanchevo-Strymon Detachment

Structural data from the basement exposed below the Strymon detachment ("Strymon basement") [*Dinter*, 1998] allow reconstruction of the detachment surface and estimation of the amount of eroded basement material. Profiles in Figures 7c and 7d across the Vrondou massif and parallel to the transport direction of the detachment (gneissic lineation mapped by *Dinter* [1998]; Figure 2 for locations of profiles) show the shallow (≤10°) southwestward dip of the detachment surface near its trace and a change to subhorizontal orientations near the crest of the gneiss dome. The amount of erosion is generally ≤200 m across most of the dome (Figures 7c and 7d); south of the Vrondou pluton, the surface of the Strymon detachment coincides with the top of a widely exposed marble layer [*Dinter*, 1998]. On the northeastern side, available structural data are insufficient to facilitate reliable reconstruction of the detachment surface. Based on these reconstructions we suggest that the Strymon basement was exhumed in the footwall of a low-angle detachment. Extension did not produce significant topographic relief and did not significantly enhance erosion of the exposed footwall.

The geometry of the GSF and the basement of the southern Pirin is less clear, and an unambiguous reconstruction of the detachment surface is not easily possible (Figure 7b). Near the contact to the Sandanski basin the footwall of the GSF is strongly weathered concealing much of its structures. The dip of the fault is steeper compared to the Strymon detachment (20–30°) [e.g., *Zagorchev*, 1992] although it may have been tilted during subsequent deformation (sections 5.5 and 5.6). The mylonitic foliation in the basement is not parallel to the contact. Away from the trace of the GSF structures (folds, gneissic foliation, mylonites, and cataclasites of the Sandanski Memorial shear zone) predate the GSF [*Jahn-Awe et al*., 2010]. Because of these structural differences between the footwall exposures of the Strymon detachment and the GSF, we suggest that the Gorno Spanchevo-Strymon detachment changes its geometry laterally: The southern (Strymon) part of the shear zone is a low-angle detachment dipping ≤10° to the SW. Horizontal offset decreases from ~75 km in the south (Symvolon region) to ~45 km in the Vrondou region (offset estimate based on 20° differential block rotation around a pole NNW of the Sandanski basin and orientation of stretching lineation throughout the basement following *Brun and Sokoutis* [2007] and paleomagnetic data by *Haubold et al*. [1997]). In the southern Pirin, horizontal offset is less than ~40 km constrained by the NE-SW distance between the western margins of the Mesta and Sandanski basins. We propose that near its northern tip the shear zone rotates to steeper dip angles as the total amount of horizontal extension decreases. The switch to steeper dip angles may be associated with a change from ductile to more brittle deformation and a strong cataclastic overprint that may account for the strong weathering observed along the GSF. Steeper dip angles of the GSF compared to the Strymon detachment imply a stronger vertical component in the motion of the GSF footwall suggesting that Miocene extension was accompanied by surface uplift. Exhumation was accomplished, in part, by denudation in response to footwall uplift rather than purely tectonic exhumation. The vicinity to the Vrondou massif 30 km farther south, which has experienced almost no erosion since the Miocene, suggests that the amount of Miocene erosion in the southern Pirin may be small, probably on the order of a few kilometers at most. If this assumption is correct, the reset ZHe ages of 13BG08 and 13BG09 reflect a combination of tectonic and erosional exhumation in the Miocene (see section 5.7 for a discussion of relief and erosion).

5.4. Sandanski Basin and Sediment Source

Detrital thermochronology from samples of the Sandanski basin provide insights into the basin evolution and potential sediment sources. Detrital ages that are as young as the depositional age of the sediment (for each sample 50% of detrital ages are <5 Ma older than depositional age) indicate an extremely short lag time; i.e., exhumation of the grains to the surface, transport, and deposition occurred within a time span shorter than the resolution of the dating method (approximately ≤2 Ma). The most likely source of the youngest grains are thus the adjacent Pirin massif, and the short lag time indicates active normal faulting and footwall exhumation by rapid erosion at the time of deposition, i.e., in the late Miocene.

Bedrock AHe ages from the southern Pirin (15.2 ± 1.7 Ma to 17.6 ± 2.0 Ma) are older than 80% of the detrital ages of both samples (mean ages 14.0 ± 2.8 and 13.2 ± 2.9 Ma; Figure 4d). Even if the current surface of the Pirin was representative of the late Miocene surface, i.e., if no erosion had occurred since then, grains that

are younger than the bedrock ages cannot be derived from the southern Pirin. The kernel smoothing functions in Figure 4d show (a) that the age distributions of both detrital samples are indistinguishable and (b) that the difference between bedrock and detrital ages cannot be attributed to the limited reproducibility of the method but that it is geologically meaningful. Therefore, the younger grains of the detrital sample, if not all sediments of the section, are derived from a source different from the southern Pirin.

Potential source regions of the detrital samples include the northern Pirin, the Ograzhden Mountains west of the graben, or a source farther north, e.g., the Rila massif. The Ograzhden massif is not known to have experienced rapid exhumation in the Cenozoic. The Rila has been exhumed in the late Miocene (13BG01: AHe 8.6 ± 1.2 Ma) and may be a source of the dated detrital material. But if material in the southern Sandanski basin is derived from as far north as the Rila, it is likely that other adjacent massifs (Osogovo, Vlahina, and Ograzhden) with early Neogene or Paleogene cooling ages [*Kounov et al*., 2004] have also contributed to the sediment budget. The general lack of AHe ages ≥20 Ma in our dated samples argues against a large source region that includes several massifs north of the Sandanski graben. Furthermore, the identical thermochronologic signal of both detrital samples suggests that the composition of the sediment remained constant between 8.1 and 7.4 Ma. This is unlikely for a large catchment area in a tectonically active area that is subject to a changing relief and potential river network reorganization. We therefore propose that the sediment source of our sample localities is more local and either comprises the entire Pirin massif or is restricted to the northern Pirin. This interpretation is in line with the sedimentological characteristics of the samples (coarse conglomerate to breccia with boulders of several cubic meters, sand lenses with an immature arcosic composition), which suggests a proximal deposition environment.

5.5. West Pirin and Melnik Faults: Geometry and Timing

If the young grains are derived from the northern Pirin, then the massif must have experienced an episode of rapid exhumation and erosion in the late Miocene that did not affect the thermochronologic record of the southern Pirin. We suggest that the West Pirin fault became active in the late Miocene leading to rapid exhumation and cooling of its footwall. Unlike the Gorno Spanchevo-Strymon detachment, the steeply dipping West Pirin fault was associated with rift flank uplift and rapid erosion of the emerging topography. In order to exhume reset AHe ages the offset must have been >2.5 km assuming a geothermal gradient of 30°C/km. This estimate is in line with *Zagorchev* [1992] who estimates a maximum offset of ~3.5 km on the West Pirin fault near Sandanski.

The oldest material eroded from the Pirin massif after initiation of the West Pirin fault is characterized by AHe cooling ages that are early to late Miocene (footwall of the GSF) or older (north of the tip of the GSF). This material that is unreset by late Miocene faulting may be preserved in the Delchevo Formation at the base of the Sandanski basin infill, or it may have bypassed the graben and transported to the Strymon or Orfanos basins (Figure 2). By 8.1 Ma (depositional age of 13BG05) faulting has already exposed reset apatites; i.e., ≥2.5 km of material has been denuded since the onset of faulting. Depending on the slip rate and efficiency of erosion, the onset of faulting was between 0.4 Ma (exhumation rate of 5 mm/yr) and 2 Ma (exhumation rate of 1 mm/yr) earlier, between ~8.5 and 10 Ma. This estimate is in agreement with biochronologic [*Spassov et al*., 2006] ages suggesting that sediment accumulation started at 10 Ma, coeval to the onset of faulting and exhumation.

Transportation pathways of the analyzed detrital samples were short. The source of the material may have been limited to one drainage basin that was sourced in the emerging northern Pirin and remained constant between 8.1 and 7.4 Ma. We conclude that with the onset of normal faulting at ~10 Ma a significant topographic relief with high, rapidly eroding mountains in the northern Pirin was formed. Normal faulting occurred continuously or episodically at least until the end of deposition of the Kalimantsi Formation as several normal faults including the Melnik fault offset Sandanski and Kalimantsi sediments, i.e., at least until ~7 Ma. It follows that the contact between the Neogene sediments in the Sandanski graben and the GSF is a depositional contact as already proposed by *Westaway* [2006].

5.6. Active Deformation Inferred From River Morphology

For a first-order scrutiny of neotectonics in SW Bulgaria we investigate regional variations in river channel steepness (Figure 5) as well as longitudinal profiles of rivers from the Pirin massif into the Sandanski basin (Figure 6).

5.6.1. New and Previous Evidence for Active Deformation

River channels that cross suspected or proven Quaternary and active faults show higher ks_n values ($\geq$150) in the footwall basement $\leq$5 km upstream of the fault trace compared to lower ks_n values (40–100) in the hanging wall (Figure 5). Although this switch in ks_n values usually corresponds to a lithologic change, we attribute the increased channel steepness to active footwall uplift based on the comparison with nearby streams that cross a similar lithologic boundary without crossing an active fault, and which do not show significant changes in ks_n value along the channel. Several examples are discussed below.

Quaternary basins that have been associated with active normal faulting include the Razlog basin and the Blagoevgrad basin bounded in the south by the Predela and Saparevo faults, respectively (Figure 5) [*Meyer et al*., 2002; *Tranos et al*., 2006]. In both cases the same lithologic contrast (basement consisting of granite and migmatitic gneiss) exists at the southern and northern basin margins. However, increased ks_n values are only detected in the basement to the south of the basins (Figure 5) suggesting that both basins are half grabens above north dipping normal faults.

The NE striking Stob fault in the southern Blagoevgrad basin (Figure 5) offsets late Miocene fluvial sediments, and Quaternary deposits are mapped north of an escarpment visible in the field [*Tranos et al*., 2006; *Tueckmantel et al*., 2008]. River morphology reflects this fault in the asymmetry of the Quaternary basin with an axial river (Rila River) closely following the fault trace (Figure 5). The Stob fault therefore represents the southwestward continuation of the Saparevo fault either as one continuous fault or as two separate en echelon segments.

The seismically active Krupnik fault (Figure 5) [*Meyer et al*., 2002] forms the southern boundary of a half graben with late Miocene to Quaternary sediments in the hanging wall. The onset of normal faulting is disputed and may be late Miocene [e.g., *Meyer et al*., 2002] or $\leq$3 Ma [e.g., *Westaway*, 2006; see also *Tranos et al*., 2006]. The fault is clearly reflected in the morphology of the Struma River, which accumulates Quaternary alluvial deposits in the hanging wall and incises granitic basement in the footwall (Kresna gorge; Figure 5). Along the Kresna gorge and several kilometers north and south of it, the Struma River is characterized by high ks_n values ($<$1000), which is likely a combination of the low erodibility of the granitic basement and tectonic uplift of the Krupnik footwall.

The E-W striking Podgorie [*Zagorchev*, 1992] and Kerkini faults [*Mountrakis et al*., 2006] (Figure 5) north and south of the Belasitsa Mountains are described as Quaternary or active normal faults. Steep river sections (ks_n 150–300) are recorded in the basement on both sides of the Belasitsa Mountains (migmatitic gneiss and granite) but not in the lithologically identical adjacent massifs to the north (Ograzhden Mountains) or south suggesting the basins are half grabens adjacent to the Belasitsa horst. In the Strumitsa basin, the axial river flows along the northern margin of the valley, Neogene strata are tilted to the north [*Zagorchev*, 1992], and large alluvial fans are shed from the south. This geometry could indicate an active normal fault north rather than south of the graben. We prefer the alternative interpretation that this geometry results from younger and/or faster offset on the Kerkini normal fault compared to the Podgorie fault thus tilting its entire footwall (Belasitsa Mountains and Strumitsa basin) toward the north.

In contrast to the Strymon basin, which forms a large Quaternary depocenter, the Sandanski basin is being actively incised (bedrock incision in the Kresna gorge in the north, Quaternary river terraces within the Sandanski Neogene deposits). We propose that the main structure accommodating this differential uplift is the Kerkini normal fault. It is mapped only west of the Struma River but may continue farther east offsetting the Strymon and Gorno Spanchevo detachments [*Mountrakis et al*., 2006]. The surface of late Miocene sediments is at approximately 700–900 m asl in the Sandanski basin and at approximately 1000 m below sea level in the Strymon basin [*Erki et al*., 1984]. If this offset results from the Kerkini fault, vertical throw may be ~1500–2000 m since the early Pleistocene (1000 m Pleistocene and Quaternary sediments in Strymon basin) [*Erki et al*., 1984].

The orientation of Quaternary normal faults ranges from NE trending (e.g., Stob and Saparevo) to E-W trending (Podgorie and Kerkini) to SE trending (Predela and West Serres faults). Correspondingly, seismicity indicates N-S extension with *T* axes varying between 315°NW and 45°NE [*Burchfiel et al*., 2000; *Kotzev et al*., 2001, 2006]. We therefore suggest that both sets of normal faults, although almost perpendicular to each other, are attributed to the same N-S extensional stress field. The variation in fault trends developing in a uniform stress field suggests that location and orientation of the faults is strongly influenced by a variable rheology of the upper crust and that some of these faults may reactivate older structures.

5.6.2. Quaternary Reactivation of NNW Trending Normal Faults

High channel steepness indices were also found in the basement along several of the NNW-SSE trending structures, e.g., on the eastern and western sides of the Pirin massif and east of the Mesta detachment (Figure 5). The patterns are generally less distinct than for the E-W trending faults. The river profile of the northernmost river from the Pirin into the Sandanski basin (Figure 6, stream A1) shows a continuous concave-up near-equilibrium profile from the source through the granitic basement and the Sandanski basin. The rivers farther south (Figure 6, streams B1 to H6) have knickpoints and knickzones approximately 2–5 km upstream of the trace of the GSF and West Pirin faults and 200–400 m above the basin surface. It is highly unlikely that knickpoints are preserved from late Miocene (West Pirin fault) or even early Miocene (GSF) faulting. The knickpoints could indicate younger (Quaternary) reactivation of the older structures. Field mapping showed that the granitic/gneissic basement in a zone a few kilometers below the surface of the GSF and West Pirin faults is cataclastic and strongly weathered, making the distinction between weathered basement and adjacent basin sediments consisting of mostly unconsolidated granitic detritus often difficult and probably causing some of the dispute about the stratigraphic or tectonic nature of the contact. We therefore suggest that the knickpoints below 1200 m asl (Figure 6) and high ks_n values in the basement (Figure 5) reflect a change in erodibility between the strongly weathered rocks near the fault trace and fresher outcrops at higher altitudes. Knickpoints at higher altitudes (H3: ~1200 m asl; D1 and G1: ~1900 m asl) are related to glacial erosion during the Last Glacial Maximum (cf. Pleistocene glacial deposits in the catchment of D1 above 1600 m asl; Figure S1).

The knickpoint in stream H1 at its intersection with the Melnik fault (Figure 6) may indicate that the Melnik fault has been active in the Quaternary. Alternatively, the knickpoint may reflect the lithological contrast between the more resistant Kalimantsi sandstones in the footwall and the strongly weathered, easily erodable syntectonic megabreccia in the hanging wall. The sedimentary record in the footwall and hanging wall of the Melnik fault and, in particular, the occurrence of syntectonic breccia not only near the surface but also at deeper stratigraphic levels suggests that the Melnik fault was active in the late Miocene as part of the West Pirin normal fault system. The West Pirin fault is locally capped by unfaulted Pleistocene sediments suggesting that it has been inactive since at least the Pleistocene. For the Melnik fault we cannot exclude the possibility that it has been reactivated in the Quaternary. Timing of the Ograzhden normal fault, which has been described as a minor normal fault with $\leq$500 m vertical offset postdating initiation of the West Pirin fault (Figure 5) [*Zagorchev*, 1992], remains elusive. The only other NW-SE trending fault that has been suggested to be recently active is the Gotse Delchev normal fault (Figure 5) [*Westaway*, 2006, and references therein], and further analysis of the river morphology may reveal neotectonic activity.

5.6.3. Quaternary Westward Tilting of the Sandanski and Strymon Basins

The southern Blagoevgrad, Sandanski, and Strymon basins are asymmetric with the active channel located in the westernmost part of the basins (Figures 2 and 5). This asymmetry may result from regional tilting of the entire area due to regional uplift farther east or subsidence farther west. Alternatively, it could indicate Quaternary or active faulting along the western basin margin (Ograzhden fault).

In the Strymon basin, normal faults are shown on geologic maps on the east and west sides of the Serres graben, but to our knowledge few studies provide detailed data on the geometry and timing of the faults (Figure 2). *Dinter* [1998] estimates onset of faulting on the West Serres fault at ~3.5 Ma and ~3.5 km vertical offset based on the thickness of Quaternary sediments [cf. *Erki et al.*, 1984; *Dinter and Royden*, 1993]. We suggest that faulting could be responsible for the apparent westward tilting of the Strymon drainage and that offset on the West Serres fault may be younger and/or higher compared to the East Serres fault.

5.7. Relief, Footwall Erosion, and Sedimentary Basins

One of the main questions of this study is the relation between sedimentary basins and extensional structures. For example, a discrepancy is reported in the literature between the early to middle Miocene age of the Strymon detachment constrained by fission track cooling ages from the footwall [*Kounov et al.*, 2015] and the middle Miocene to Pliocene and Quaternary sediments in the Strymon Valley [*Erki et al.*, 1984], which led early workers to underestimate of the age of the shear zone [*Dinter and Royden*, 1993]. A similar dispute exists about the exhumation of the Thassos Island core complex in the southern continuation of the Strymon detachment (Figure 1). Here ductile core complex-type exhumation in the Oligocene to middle Miocene (26–13 Ma) is followed by brittle normal faulting and development of the late Pliocene to Pleistocene Limenaria basin west of the island [*Wawrzenitz and Krohe*, 1998; *Brun and Sokoutis*, 2007].

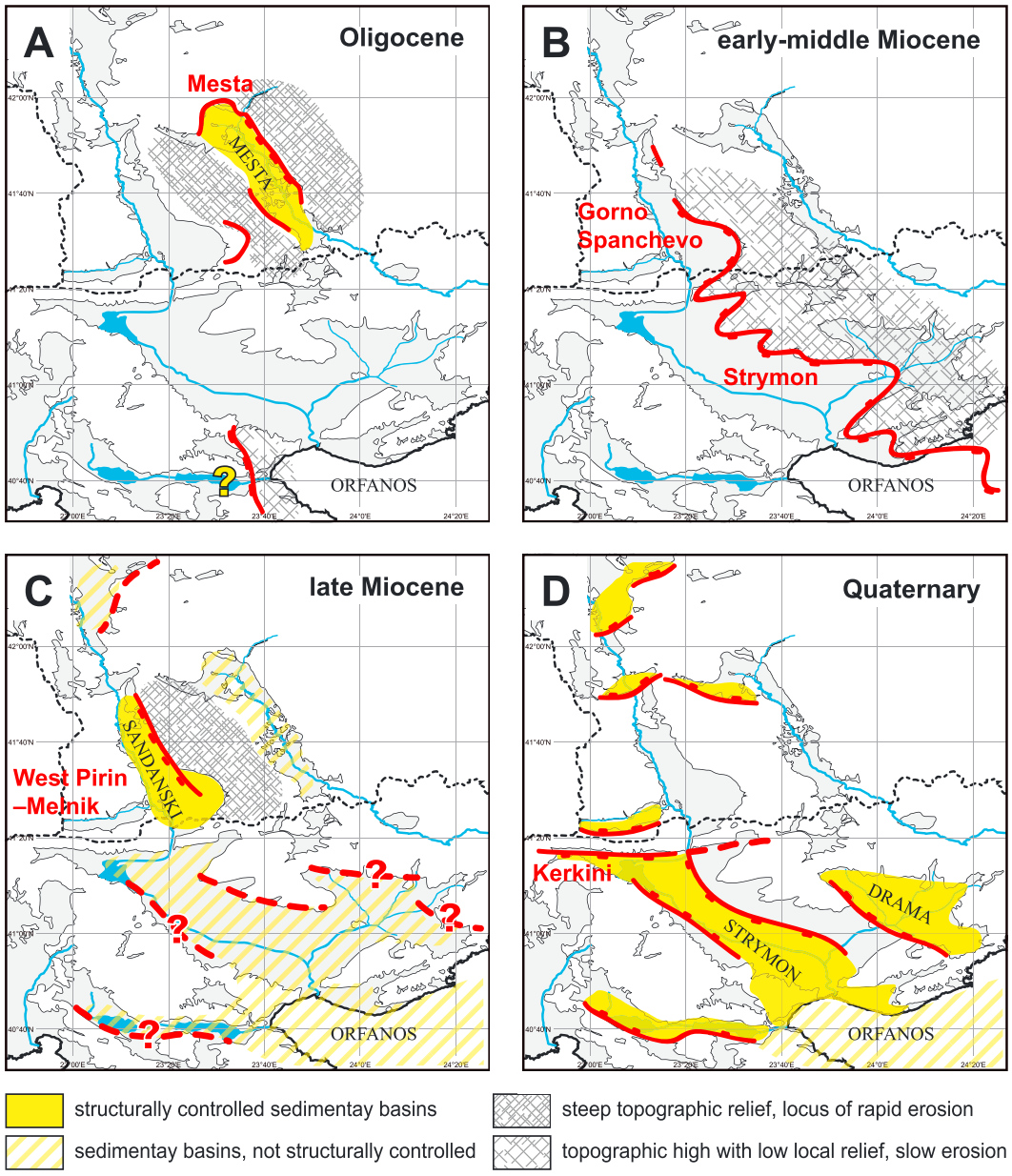

Figure 8. Summary of Cenozoic structural, sedimentary, and topographic evolution of the SRCC. (a) Eocene-Oligocene ENE-WSW extension was accommodated by the Mesta and Kerdilion detachments. Other Paleogene detachments that have been identified NW of our study area are not included. The Mesta detachment is associated with a volcanic-sedimentary basin in its hanging wall. Source of the sediments is probably the eastern footwall as well as the exhumed footwall in the Pirin. No Paleogene basin is preserved for the Kerdilion detachment, either because low-angle detachment faulting did not result in high topographic relief and development of a sediment basin or the basin was eroded subsequently, e.g., during late Miocene-Pliocene extension [*Georgiev et al.*, 2010]. (b) The early to middle Miocene Strymon low-angle detachment did not create significant relief or result in enhanced erosion and basin formation. Near its northern tip, the steeper Gorno Spanchevo segment of the detachment may have resulted in some relief and erosion but no corresponding sediment deposits have been detected. The southern part of the Strymon detachment was probably active until the late Miocene (7 Ma). (c) NE-SW extension in the late Miocene resulted in localized development of a half graben and rift shoulder in SW Bulgaria (Sandanski basin and Pirin massif). In the southern SRCC extension may have been distributed over several structures, which are not well documented. Relatively small offsets on individual faults resulted in little topographic relief and no well-defined structurally controlled basins. (d) The largest Quaternary basins are located in northern Greece (Strymon, Drama, and Orfanos basins) and are bound by NW-SE trending normal faults as well as the E-W trending Kerkini fault. Smaller basins exist above approximately E-W trending normal faults in SW Bulgaria.

Whereas *Wawrzenitz and Krohe* [1998] propose that a high and rapidly eroding relief developed in the early to middle Miocene as a result of isostatic uplift of the dome (AFT ages 15–8 Ma), *Brun and Sokoutis* [2007] attribute rapid erosion and basin formation to steep normal faulting in the late Pliocene-Pleistocene.

A number of reasons are conceivable to explain the lack of synkinematic sediments above normal faults and shear zones:

1. Synkinematic strata may have been deposited but eroded subsequently, e.g., due to a later episode of regional uplift.
2. Sediment eroded from the uplifted footwall may have bypassed the locally developing rift basin if transport and deposition were controlled by a significantly lower base level farther away.
3. Extension may not have created significant relief or enhanced footwall erosion, for example, if the extensional structure dips at a shallow angle.

Figure 8 summarizes the structural and sedimentary evolution of the SRCC since the Oligocene. Eocene-Oligocene extension and basin formation has been studied in most detail in the Mesta region. Faulting on the Mesta detachment was accompanied by footwall erosion and formation of a synkinematic basin filled with Paleogene volcanic, volcaniclastic, and clastic deposits [e.g., *Burchfiel et al*., 2003] (Figure 8a). The Mesta graben and detachment are different from the other Cenozoic structures in the SRCC in that the footwall was exhumed on both sides of the graben assisted by brittle normal faults (Dobrotino and Breznitsa faults) [*Georgiev et al*., 2010] broadly coeval to detachment faulting. Further analysis is necessary to unravel the cause for this geometry, which could be, for example, a particularly hot and weak upper crust resulting from widespread decompression melting in the early Cenozoic [*Rey et al*., 2009]. Less is known about the Kerdilion detachment, its geometry, and potential association with a synrift basin, although *Georgiev et al*. [2010] speculate that a synextension basin existed but has subsequently been eroded.

In the middle Miocene, the Strymon basement was exhumed along a low-angle detachment [*Kounov et al*., 2015] (Figure 8b). Although some tilting or uplift/subsidence is likely to have occurred since then, e.g., on the East and West Serres and Kerkini normal faults (section 5.6) in addition to an unknown amount of regional uplift/subsidence and absolute sea level change, we suggest that the current detachment geometry ($\leq$10° dip to the WSW) and the elevation difference between the crest of the dome (~1800 m asl) and its western margin (~200 m asl) is similar to the topography at the end of detachment faulting in the middle to late Miocene (Figures 7c and 7d). The landscape resulting from detachment faulting was thus characterized by gentle slopes ($\leq$10°) and a moderate relief (~1500 m) over long wavelengths (30–50 km). The amount of erosion since the late Miocene is $\leq$0.2 km amounting to an average erosion rate $<$0.02 mm/yr.

North of the Greek-Bulgarian border the Strymon detachment ends laterally. Closer to its termination in the Pirin massif the dip of the shear zone rotates to steeper angles (GSF segment of the shear zone, $\leq$30°). The Oligocene ZHe age of 13BG012 constrains the amount of erosion since the middle Miocene to $<$6 km (section 5.2). Taking into account $>$2.5 km of late Miocene exhumation (West Pirin fault, section 5.5) in addition to possibly $>$1.5 km Pleistocene and younger offset on the Kerkini fault (section 5.6) and considering the proximity to the low-angle Strymon segment above the Vrondou massif, we speculate that the surface uplift resulting from the early to middle Miocene GSF and hence the amount of footwall erosion was not significantly higher than in the Vrondou massif. Consequently, no large sedimentary basin developed in the hanging wall of the GSF (Figure 8b).

Detachment faulting was overprinted by the West Pirin normal fault starting at 10 Ma (section 5.5). Late Miocene normal faulting resulted in footwall uplift by at least 2.5 km in the northern Pirin (reset detrital AHe ages) and a lesser amount in the southern Pirin (unreset AHe bedrock ages). Rift flank uplift along steeply dipping faults created a high local relief across the fault scarp and resulted in steep hillslopes. Because of the steep topography, surface uplift was compensated by rapid erosion and voluminous proximal deposition in the emerging Sandanski basin (Figure 8c). While the West Pirin fault became active in the northern SRCC low-angle detachment, faulting was probably still going on in the southern SRCC (7–10 Ma AFT and 12.3 Ma ZFT ages in the Symvolon massif; Figure 2). Although the GSF and West Pirin fault represent distinguishable episodes of extension in SW Bulgaria, they probably belong to one continuous Miocene phase of regional extension.

Late Miocene sediments in the Strymon and Drama basins suggest that steep normal faults may also have overprinted the southern part of the SRCC contemporaneously to the West Pirin fault. However, no major late

Miocene normal faults have been unambiguously identified in the field, and there is no evidence of intense late Miocene erosion of basement exposure in the southern SRCC. There is no low-temperature thermochronology data available from the basement outcrop southwest of the Strymon basin to evaluate the amount and timing of its Cenozoic exhumation. In contrast to the localized extension, uplift, and erosion in the northern Pirin ("narrow rift"), we propose that late Miocene extension in the southern SRCC was distributed over a wide area and several normal faults with vertical offsets $\leq$1 km with relatively minor effects on topographic relief, erosion, and deposition ("wide rift"; Figure 8c). Possible reasons for the differences in the mode of late Miocene rifting between northern and southern SRCC include lateral variations in the tectonic stress field, e.g., distance to the North Anatolian fault zone, and presence of preexisting structures that become reactivated. The mode of rifting may also reflect differences in the thermal state of the upper crust [e.g., *Tirel et al*., 2006; *Rey et al*., 2009] resulting from scissor-like opening of the SRCC with 75–120 km of stretching in the southern part [*Brun and Sokoutis*, 2007; *Georgiev et al*., 2010; this study] likely resulting in a hotter and rheologically weak crust compared to the less intensely stretched northern part.

The modern topography and Quaternary structures are key to understanding the past evolution of normal faults, relief, and sediment basins. Quaternary approximately N-S extension is reflected in steeply dipping normal faults associated with hanging wall basins (Figure 8d). One of the most significant Quaternary normal faults is the Kerkini fault, which uplifts SW Bulgaria relative to the Strymon basin, a large, structurally controlled basin with ~1000 m Quaternary basin infill [*Erki et al*., 1984]. By comparison Quaternary basins in SW Bulgaria are small. Although these faults obviously produced some topographic relief and enhance erosion of their footwall, exhumation $<$1 km is generally not detectable in bedrock low-temperature thermochronology. We envision that these basins have little potential to be preserved over longer timescales (several million years) unless they evolve into lager half grabens comparable to the Sandanski basin. The Quaternary normal faults in SW Bulgaria and the associated basins and topography may thus be a modern analog for late Miocene extension in the southern SRCC.

Some of the Quaternary faults may be listric and connect with a sole detachment at depth. If extension continues, the footwall may evolve into a metamorphic gneiss dome bound by a low-angle detachment similar to the Strymon detachment. After several tens of kilometers of extension, the uppermost part of the structure, i.e., the steep normal fault and associated Quaternary basin, may be removed by erosion. We speculate that the Quaternary normal faults and basins may also be an analog for the onset of early to middle Miocene extension on the Strymon detachment and that small brittle normal faults and basins existed on the east side of the Strymon basement. The main difference between detachment faulting in the early to middle Miocene (Figure 8b) and brittle faulting in the late Miocene (Figure 8c) is the larger amount of crustal stretching accommodated during the earlier episode.

Our analysis of normal faulting, erosion, and basin formation in SW Bulgaria reveals that late Miocene E-W extension accommodated by the steeply dipping West Pirin fault resulted in high local relief leading to rapid erosion of the footwall and voluminous proximal deposition in the Sandanski basin. The late Miocene topographic relief in SW Bulgaria was thus probably steeper compared to the early to middle Miocene and compared to today. The Pikermian Biome mammal faunas populating SW Bulgaria and northern Greece between 9 and 7 Ma flourished in a landscape of steep topographic relief. The developing mountains may have influenced atmospheric circulation, increased orographic precipitation, and created new habitats [*Hoorn et al*., 2013], which may partly explain differences in mammalian communities within the Pikermian Biome (e.g., between the Balkans and Anatolia) [*Kostopolos*, 2009], including the presence of hominids in the Upper Thrace basin of Central Bulgaria [*Spassov et al*., 2012].

6. Synthesis and Relationship of Normal Faulting to Basin Formation

The Pirin Mountains are the northernmost part of the South Rhodope core complex (SRCC). Cenozoic extension occurred in at least three stages (Figures 8a–8c):

1. Eocene/Oliocene ENE-WSW extension (Mesta detachment and Breznitsa and Dobrotino normal faults) led to rapid exhumation of synextensional plutons (e.g., Teshovo pluton). This phase ended shortly after 28 Ma (28.1 ± 1.6 Ma ZHe age of Teshovo pluton).

2. Rapid exhumation and cooling in the early to middle Miocene (circa 18–15 Ma) was controlled by the Gorno Spanchevo fault, the northernmost segment of the Strymon low-angle detachment, which exhumed rocks from ≥6 km depth (15.2 to 15.5 Ma ZHe ages).
3. The West Pirin normal fault became active at 10 Ma leading to rift flank uplift, footwall erosion, and formation of the Sandanski half graben. The amount of erosional exhumation was ≥2.5 km in the northern and central Pirin and ≤1–2 km in the southern Pirin (bedrock and detrital AHe ages). Intrabasin faults including the Melnik fault belong to the same late Miocene set of normal faults and were active during deposition of the Sandanski basin sediments. Although in SW Bulgaria the GSF and West Pirin fault system represent distinguishable deformation phases, on a regional scale early to late Miocene extension was probably continuous and accommodated by the Strymon detachment.

The youngest phase of deformation comprises westward tilting, either regionally or accommodated by the Ograzhden and West Serres normal faults, and active ~N-S extension resulting in formation of several Quaternary fault-bounded basins. The most significant Quaternary normal fault is the E-W striking Kerkini fault, which uplifted the Sandanski basin relative to the Strymon basin.

Low-angle detachments can accommodate several tens of kilometers of horizontal stretching. Footwall exhumation of low-angle detachments can expose footwall rocks in a topographic high of >1000 m above the surrounding areas, but if the detachment dips at a shallow angle (≤10°), the resulting slopes are gentle and may not significantly enhance footwall erosion. An example for low-angle detachment faulting is the middle Miocene Strymon detachment in northern Greece, which resulted in a landscape characterized by moderate relief (~1500 m) and long wavelengths (30–50 km). Detachment faulting did not enhance footwall erosion, and no significant synkinematic sedimentary basin was developed in the hanging wall.

In contrast, steeply dipping brittle normal faults (≥60°) associated with mostly vertical movement of the footwall lead to rift flank uplift and create a high local relief across the fault scarp. The resulting topography is characterized by steep slopes and short wavelengths and is subject to rapid erosion. Eroded material is deposited in an emerging hanging wall basin, although some material may be transferred to a lower base level farther away. Examples for steep normal faults include ~E-W trending Quaternary faults throughout SW Bulgaria and the SRCC and the late Miocene West Pirin fault. These brittle faults are associated with hanging wall sedimentary basins including the late Miocene Sandanski basin.

Apart from a climate control on erosion and deposition, the presence or absence of sedimentary basins in the hanging wall of extensional structures and possible time gaps between the onset of extension and the age of the oldest synkinematic deposits are thus controlled by the geometry of the fault and the relative amounts of vertical and horizontal movements on the fault. In the SRCC, the different Cenozoic episodes of extension and their respective geomorphic and structural expressions reflect variable amounts of extension (several tens of kilometers of horizontal stretching on the Strymon low-angle detachment versus mostly vertical movement on the West Pirin fault) but are probably also affected by the rheological and thermal structure of the crust (possibly reflected in late Miocene narrow rifting in the Sandanski basin versus wide rifting in the southern SRCC).

Acknowledgments
We thank Tzanko Tzankov (University of Blagoevgrad) and Nikolai Spassov (National Museum of Natural History, Sofia) for guiding us in the field. Special thanks for helping with the setup of the U-Th-Sm thermochronology facilities at the University of Tübingen go to Peter Reiners (University of Arizona), James Metcalf (University of Colorado Boulder), and Ilka Schönberg and Elmar Reiter (University of Tübingen). We also thank Jan Pleuger and an anonymous reviewer for their thorough and constructive reviews. Data are published in the supporting information.

References

Armijo, R., B. Meyer, A. Hubert, and A. Barka (1999), Westward propagation of the North Anatolian fault into the northern Aegean: Timing and kinematics, *Geology*, *27*(3), 267–270.

Beratan, K. K. (Ed) (1996), *Reconstructing the History of Basin and Range Extension Using Sedimentology and Stratigraphy*, *Geol. Soc. Am. Spec. Pap.*, vol. 303, Geol. Soc. of Am., Boulder, Colo.

Bernor, R. L. (1984), A zoogeographic theater and a biochronologic play: The time/biofacies phenomena of Eurasian and African Miocene mammal provinces, *Paléobiol. Continentale*, *14*, 121–142.

Bornovas, J., and T. Rondogianni-Tsiambaou (1983), Geological map of Greece 1:500.000, Athens, Greece.

Boulton, S. J., and A. C. Whittaker (2009), Quantifying the slip rates, spatial distribution and evolution of active normal faults from geomorphic analysis: Field examples from an oblique-extensional graben, southern Turkey, *Geomorphology*, *104*(3), 299–316.

Bozkurt, E., and H. Sözbilir (2004), Tectonic evolution of the Gediz Graben: Field evidence for an episodic, two-stage extension in western Turkey, *Geol. Mag.*, *141*(1), 63–79, doi:10.1017/S0016756803008379.

Brun, J. P., and D. Sokoutis (2007), Kinematics of the southern Rhodope core complex (North Greece), *Int. J. Earth Sci.*, *96*(6), 1079–1099.

Burchfiel, B. C., R. Nakov, T. Tzankov, and L. H. Royden (2000), Cenozoic extension in Bulgaria and northern Greece: The northern part of the Aegean extensional regime, *Geol. Soc. London, Spec. Publ.*, *173*(1), 325–352.

Burchfiel, B. C., R. Nakov, and T. Tzankov (2003), Evidence from the Mesta half-graben, SW Bulgaria, for the Late Eocene beginning of Aegean extension in the Central Balkan Peninsula, *Tectonophysics*, *375*(1), 61–76.

Burchfiel, B. C., R. W. King, A. Todosov, V. Kotzev, N. Durmurdzanov, T. Serafimovski, and B. Nurce (2006), GPS results for Macedonia and its importance for the tectonics of the Southern Balkan extensional regime, *Tectonophysics*, *413*(3), 239–248.
Burchfiel, B. C., R. Nakov, N. Dumurdzanov, D. Papanikolaou, T. Tzankov, T. Serafimovski, R. W. King, V. Kotzev, A. Todosov, and B. Nurce (2008), Evolution and dynamics of the Cenozoic tectonics of the South Balkan extensional system, *Geosphere*, *4*(6), 919–938.
Chen, Z., Y. Liu, K. V. Hodges, B. C. Burchfiel, L. H. Royden, and C. Deng (1990), The Kangmar Dome: A metamorphic core complex in southern Xizang (Tibet), *Science*, *250*(4987), 1552–1556.
Coney, P. J., and T. A. Harms (1984), Cordilleran metamorphic core complexes: Cenozoic extensional relics of Mesozoic compression, *Geology*, *12*(9), 550–554.
Cyr, A., D. Granger, V. Olivetti, and P. Molin (2010), Quantifying rock uplift rates using channel steepness and cosmogenic nuclide-determined erosion rates: Examples from northern and southern Italy, *Lithosphere*, *2*, 188–198.
Davis, G. H., and P. J. Coney (1979), Geologic development of the Cordilleran metamorphic core complexes, *Geology*, *7*(3), 120–124.
De Bonis, L., G. Bouvrain, D. Geraads, and G. Koufos (1992), Diversity and paleoecology of Greek late Miocene mammalian faunas, *Palaeogeogr. Palaeoclimatol. Palaeoecol.*, *91*, 99–121.
Densmore, A. L., N. H. Dawers, S. Gupta, R. Guidon, and T. Goldin (2004), Footwall topographic development during continental extension, *J. Geophys. Res.*, *109*, F03001, doi:10.1029/2003JF000115.
Densmore, A. L., N. H. Dawers, S. Gupta, and R. Guidon (2005), What sets topographic relief in extensional footwalls?, *Geology*, *33*(6), 453–456.
Dinter, D. A. (1998), Late Cenozoic extension of the Alpine collisional orogen, northeastern Greece: Origin of the north Aegean basin, *Geol. Soc. Am. Bull.*, *110*, 1208–1230.
Dinter, D. A., and L. H. Royden (1993), Late Cenozoic extension in northeastern Greece: Strymon Valley detachment system and Rhodope metamorphic core complex, *Geology*, *21*(1), 45–48.
Dumurdzanov, N., T. Serafimovski, and B. C. Burchfiel (2005), Cenozoic tectonics of Macedonia and its relation to the South Balkan extensional regime, *Geosphere*, *1*(1), 1–22, doi:10.1130/GES00006.1.
Duvall, A., E. Kirby, and D. Burbank (2004), Tectonic and lithologic controls on bedrock channel profiles and processes in coastal California, *J. Geophys. Res.*, *109*, F03002, doi:10.1029/2003JF000086.
Erki, I., N. Kolios, and L. Stegena (1984), Heat-flow density determination in the Strymon basin, NE Greece, *J. Geophys.*, *54*(2), 106–109.
Farley, K. A. (2002), (U-Th)/He dating: Techniques, calibrations, and applications, *Rev. Mineral. Geochem.*, *47*(1), 819–844.
Finnegan, N., G. Roe, D. Montgomery, and B. Hallet (2005), Controls on the channel width of rivers: Implications for modeling fluvial incision of bedrock, *Geology*, *33*, 229–232.
Flint, J. (1974), Stream gradient as a function of order magnitude and discharge, *Water Resour. Res.*, *10*, 969–973, doi:10.1029/WR010i005p00969.
Friedmann, S. J., and D. W. Burbank (1995), Rift basins and supradetachment basins: Intracontinental extensional end-members, *Basin Res.*, *7*, 109–127.
Gautier, P., and J.-P. Brun (1994), Crustal-scale geometry and kinematics of late-orogenic extension in the central Aegean (Cyclades and Evvia Island), *Tectonophysics*, *238*, 399–424, doi:10.1016/0040-1951(94)90066-3.
Gautier, P., J.-P. Brun, and L. Jolivet (1993), Structure and kinematics of Upper Cenozoic extensional detachment on Naxos and Paros (Cyclades Islands, Greece), *Tectonics*, *12*(5), 1180–1194, doi:10.1029/93TC01131.
Georgiev, N., J. Pleuger, N. Froitzheim, S. Sarov, S. Jahn-Awe, and T. J. Nagel (2010), Separate Eocene–Early Oligocene and Miocene stages of extension and core complex formation in the Western Rhodopes, Mesta Basin, and Pirin Mountains (Bulgaria), *Tectonophysics*, *487*(1), 59–84, doi:10.1016/j.tecto.2010.03.009.
Haubold, H., R. Scholger, D. Kondopoulou, and H. J. Mauritsch (1997), New paleomagnetic results from the Aegean extensional province, *Geol. Mijnbouw*, *76*, 45–55.
Hejl, E., M. Bernroider, O. Parlak, and H. Weingartner (2010), Fission-track thermochronology, vertical kinematics, and tectonic development along the western extension of the North Anatolian Fault zone, *J. Geophys. Res.*, *115*, B10407, doi:10.1029/2010JB007402.
Hinsbergen, D. J. J. (2010), A key extensional metamorphic complex reviewed and restored: The Menderes Massif of western Turkey, *Earth Sci. Rev.*, *102*, 60–76, doi:10.1016/j.earscirev.2010.05.005.
Hoorn, C., V. Mosbrugger, A. Mulch, and A. Antonelli (2013), Biodiversity of mountain building, *Nat. Geosci.*, *6*, 154.
Hourigan, J. K., P. W. Reiners, and M. T. Brandon (2005), U-Th zonation-dependent alpha-ejection in (U-Th)/He chronometry, *Geochim. Cosmochim. Acta*, *69*(13), 3349–3365.
Jahn-Awe, S., N. Froitzheim, T. J. Nagel, D. Frei, N. Georgiev, and J. Pleuger (2010), Structural and geochronological evidence for Paleogene thrusting in the western Rhodopes, SW Bulgaria: Elements for a new tectonic model of the Rhodope Metamorphic Province, *Tectonics*, *29*, TC3008, doi:10.1029/2009TC002558.
Jolivet, L., and J. P. Brun (2010), Cenozoic geodynamic evolution of the Aegean, *Int. J. Earth Sci.*, *99*(1), 109–138.
Jolivet, L., E. Lecomte, B. Huet, Y. Denèle, O. Lacombe, L. Labrousse, L. le Pourhiet, and C. Mehl (2010), The north cycladic detachment system, *Earth Planet. Sci. Lett.*, *289*, 87–104, doi:10.1016/j.epsl.2009.10.032.
Kirby, E., and K. Whipple (2001), Quantifying differential rock-uplift rates via stream profile analysis, *Geology*, *29*, 415–418.
Klimov, I., R. Marinova, A. Marinova, and I. Petrov (2010), Geological map of the People's Republic of Bulgaria and explanatory notes, 1:50.000 series Sandanski and Katuntsi sheets. Geological Institute, Bulgarian Academy of Sciences, Sofia.
Kojumdgieva, E., I. Nikolov, P. Nedjalkov, and A. Busev (1982), Stratigraphy of the Neogene in Sandanski graben, *Geol. Balc.*, *12*(3), 69–81.
Korup, O., and D. R. Montgomery (2008), Tibetan Plateau river incision inhibited by glacial stabilization of the Tsangpo gorge, *Nature*, *455*, 786–789, doi:10.1038/nature07322.
Kostopolos, D. S. (2009), The Pikermian event: Temporal and spatial resolution of the Turolian large mammal fauna in SE Europe, *Palaeogeogr. Palaeoclimatol. Palaeoecol.*, *274*, 82–95.
Kotzev, V., R. Nakov, B. C. Burchfiel, R. King, and R. Reilinger (2001), GPS study of active tectonics in Bulgaria: Results from 1996 to 1998, *J. Geodyn.*, *31*(2), 189–200.
Kotzev, V., R. Nakov, T. Georgiev, B. C. Burchfiel, and R. W. King (2006), Crustal motion and strain accumulation in western Bulgaria, *Tectonophysics*, *413*(3), 127–145.
Kounov, A., D. Seward, D. Bernoulli, J. P. Burg, and Z. Ivanov (2004), Thermotectonic evolution of an extensional dome: The Cenozoic Osogovo–Lisets core complex (Kraishte zone, western Bulgaria), *Int. J. Earth Sci.*, *93*(6), 1008–1024.
Kounov, A., E. Wüthrich, D. Seward, J. P. Burg, and D. Stockli (2015), Low-temperature constraints on the Cenozoic thermal evolution of the Southern Rhodope Core Complex (Northern Greece), *Int. J. Earth Sci.*, 1–16.
Krohe, A., and E. Mposkos (2002), Multiple generations of extensional detachments in the Rhodope Mountains (northern Greece): Evidence of episodic exhumation of high-pressure rocks, *Geol. Soc. London, Spec. Publ.*, *204*, 151–178.

Kuhlemann, J., E. Gachev, A. Gikov, S. Nedkov, I. Krumrei, and P. Kubik (2013), Glaciation in the Rila Mountains (Bulgaria) during the last glacial maximum, *Quat. Int.*, *293*, 51–62.
Kydonakis, K., J. P. Brun, and D. Sokoutis (2015), North Aegean core complexes, the gravity spreading of a thrust wedge, *J. Geophys. Res. Solid Earth*, *120*, 595–616, doi:10.1002/2014JB011601.
Lavé, J., and J. P. Avouac (2001), Fluvial incision and tectonic uplift across the Himalayas of central Nepal, *J. Geophys. Res.*, *106*(B11), 26,561–26,591, doi:10.1029/2001JB000359.
Lister, G. S., and G. A. Davis (1989), The origin of metamorphic core complexes and detachment faults formed during Tertiary continental extension in the northern Colorado River region, USA, *J. Struct. Geol.*, *11*(1), 65–94.
Loget, N., and J. van den Driessche (2009), Wave train model for knickpoint migration, *Geomorphology*, *106*, 376–382.
McClaughry, J. D., and D. R. Gaylord (2005), Middle Eocene sedimentary and volcanic infilling of an evolving supradetachment basin: White Lake Basin, south-central British Columbia, *Can. J. Earth Sci.*, *42*(1), 49–66.
McClusky, S., S. Balassanian, A. Barka, C. Demir, S. Ergintav, I. Georgiev, and G. Veis (2000), GPS constraints on plate motions and deformations in eastern Mediterranean and Caucasus, *J. Geophys. Res.*, *105*, 5695–5719, doi:10.1029/1999JB900351.
Mercier, J. L., D. Sorel, P. Vergely, and K. Simeakis (1989), Extensional tectonic regimes in the Aegean basins during the Cenozoic, *Basin Res.*, *2*(1), 49–71.
Meyer, B., R. Armijo, and D. Dimitrov (2002), Active faulting in SW Bulgaria: Possible surface rupture of the 1904 Struma earthquakes, *Geophys. J. Int.*, *148*(2), 246–255.
Mountrakis, D., M. D. Tranos, C. Papazachos, E. Thomaidou, E. Karagianni, and D. Vamvakaris (2006), Neotectonic and seismological data concerning major active faults, and the stress regimes of Northern Greece, *Geol. Soc. London, Spec. Publ.*, *260*, 649–670.
Oner, Z., and Y. Dilek (2011), Supradetachment basin evolution during continental extension: The Aegean province of western Anatolia, Turkey, *Geol. Soc. Am. Bull.*, *123*(11–12), 2115–2141.
Ouimet, W., K. X. Whipple, and D. Granger (2009), Beyond threshold hillslope: Channel adjustment to base-level fall in tectonically active mountain ranges, *Geology*, *37*, 579–582.
Papanikolaou, D. J., and L. H. Royden (2007), Disruption of the Hellenic arc: Late Miocene extensional detachment faults and steep Pliocene-Quaternary normal faults—Or what happened at Corinth?, *Tectonics*, *26*, TC5003, doi:10.1029/2006TC002007.
Ratschbacher, L., W. Frisch, F. Neubauer, S. M. Schmid, and J. Neugebauer (1989), Extension in compressional orogenic belts: The Eastern Alps, *Geology*, *17*(5), 404–407.
Reiners, P. W., T. L. Spell, S. Nicolescu, and K. A. Zanetti (2004), Zircon (U-Th)/He thermochronometry: He diffusion and comparisons with $^{40}Ar/^{39}Ar$ dating, *Geochim. Cosmochim. Acta*, *68*(8), 1857–1887, doi:10.1016/j.gca.2003.10.021.
Reinhardt, L., P. Bishop, T. B. Hoey, T. J. Dempster, and D. C. W. Sanderson (2007), Quantification of the transient response to base-level fall in a small mountain catchment: Sierra Nevada, southern Spain, *J. Geophys. Res.*, *112*, F03S05, doi:10.1029/2006JF000524.
Rey, P. F., C. Teyssier, and D. L. Whitney (2009), The role of partial melting and extensional strain rates in the development of metamorphic core complexes, *Tectonophysics*, *477*(3), 135–144.
Ring, U., T. Brachert, and C. Fassoulas (2001), Middle Miocene graben development in Crete and its possible relation to large-scale detachment faults in the southern Aegean, *Terra Nova*, *13*(4), 297–304.
Ring, U., J. Glodny, T. Will, and S. Thomson (2010), The Hellenic subduction system: High-pressure metamorphism, exhumation, normal faulting, and large-scale extension, *Annu. Rev. Earth Planet. Sci.*, *38*, 45–76.
Royden, L. H. (1993), Evolution of retreating subduction boundaries formed during continental collision, *Tectonics*, *12*(3), 629–638, doi:10.1029/92TC02641.
Royden, L. H., and D. J. Papanikolaou (2011), Slab segmentation and late Cenozoic disruption of the Hellenic arc, *Geochem. Geophys. Geosyst.*, *12*, Q03010, doi:10.1029/2010GC003280.
Safran, E. B., P. Bierman, R. Aalto, T. Dunne, K. X. Whipple, and M. Caffe (2005), Erosion rates driven by channel network incision in the Bolivian Andes, *Earth Surf. Processes Landforms*, *30*, 1007–1024.
Sklar, L., and W. E. Dietrich (1998), River longitudinal profiles and bedrock incision models: Stream power and the influence of sediment supply, in *Rivers Over Rock: Fluvial Processes in Bedrock Channels*, edited by K. J. Tinkler and E. E. Wohl, pp. 237–260, AGU, Washington, D. C.
Solounias, N., J. M. Plavcan, J. Quade, and L. Witmer (1999), The paleoecology of the Pikermian Biome and the savanna myth, in *The Evolution of Neogene Terrestrial Ecosystem in Europe, Hominoid Evolution and Climatic Change in Europe*, vol. 1, edited by J. Agusti, L. Rook, and P. Andrews, pp. 436–453, Cambridge Univ. Press, Cambridge, U. K.
Spassov, N. (2002), The Turolian Megafauna of West Bulgaria and the character of the Late Miocene "Pikermian biome", *B Soc. Paleontol. Ital.*, *41*(1), 69–81.
Spassov, N., T. Tsankov, and D. Geraads (2006), Late Neogene stratigraphy, biochronology, faunal diversity and environments of South-West Bulgaria (Struma River Valley), *Geodiversitas*, *28*(3), 477–498.
Spassov, N., D. Geraads, L. Hristova, G. N. Markov, G. Merceron, T. Tzankov, K. Stoyanov, M. Böhme, and A. Dimitrova (2012), A hominid tooth from Bulgaria: The last pre-human hominid of continental Europe, *J. Human Evol.*, *62*(2), 138–145.
Stübner, K., L. Ratschbacher, D. Rutte, K. Stanek, V. Minaev, M. Wiesinger, and R. Gloaguen (2013), The giant Shakhdara migmatitic gneiss dome, Pamir, India-Asia collision zone: 1 Geometry and kinematics, *Tectonics*, *32*, 948–979, doi:10.1002/tect.20057.
Tirel, C., J. P. Brun, and D. Sokoutis (2006), Extension of thickened and hot lithospheres: Inferences from laboratory modeling, *Tectonics*, *25*, TC1005, doi:10.1029/2005TC0011804.
Tranos, M. D., V. G. Karakosts, E. E. Papadimitriou, V. N. Kachev, B. K. Ranguelov, and D. K. Gospodinov (2006), Major active faults of SW Bulgaria: Implications of their geometry, kinematics and the regional active stress regime, *Geol. Soc. London, Spec. Publ.*, *260*, 671–687.
Tueckmantel, C., S. Schmidt, M. Neisen, N. Georgiev, T. J. Nagel, and N. Froitzheim (2008), The Rila-Pastra normal fault and multi-stage extensional unroofing in the Rila Mountains (SW Bulgaria), *Swiss J. Geosci.*, *101*(1), 295–310.
VanLaningham, S., A. Meigs, and C. Goldfinger (2006), The effects of rock uplift and rock resistance on river morphology in a subduction zone forearc, Oregon, USA, *Earth Surf. Processes Landforms*, *31*(10), 1257–1279, doi:10.1002/esp.1326.
Wawrzenitz, N., and A. Krohe (1998), Exhumation and doming of the Thassos metamorphic core complex (S Rhodope, Greece): Structural and geochronological constrains, *Tectonophysics*, *285*, 301–312.
Wernicke, B. (1981), Low-angle normal faults in the Basin and Range Province: Nappe tectonics in an extending orogen, *Nature*, *291*, 645–648.
Westaway, R. (2006), Late Cenozoic extension in SW Bulgaria: A synthesis, *Geol. Soc. London, Spec. Publ.*, *260*(1), 557–590.
Whipple, K. (2004), Bedrock rivers and the geomorphology of active orogens, *Annu. Rev. Earth Planet. Sci.*, *32*, 151–185.
Whipple, K., and G. Tucker (1999), Dynamics of the stream-power model: Implications for the height limits of mountain ranges, landscape response timescales and research needs, *J. Geophys. Res.*, *104*, 17,661–17,674, doi:10.1029/1999JB900120.

Whipple, K. X., C. Wobus, E. Kirby, B. Crosby, and D. Sheehan (2007), New tools for quantitative geomorphology: Extraction and interpretation of stream profiles from digital topographic data, Short Course presented at the Geological Society of America Annual Meeting, Denver, Colo. [Available at http://www.geomorphtools.org.]

Whitney, D. L., C. Teyssier, P. Rey, and W. R. Buck (2013), Continental and oceanic core complexes, *Geol. Soc. Am. Bull.*, *125*(3–4), 273–298.

Whittaker, A. C. (2012), How do landscapes record tectonics and climate?, *Lithosphere*, *4*(2), 160–164.

Whittaker, A., P. Cowie, M. Attal, G. Tucker, and G. Roberts (2007), Bedrock channel adjustment to tectonic forcing: Implications for predicting river incision rates, *Geology*, *35*, 103–106.

Wobus, C. W., K. X. Whipple, E. Kirby, N. P. Snyder, J. Johnson, K. Spyropolou, B. T. Crosby, and D. Sheehan (2006), Tectonics from topography: Procedures, promise and pitfalls, in *Tectonics, Climate and Landscape Evolution*, *Geol. Soc. Am., Spec. Pap.*, vol. 398, edited by S. D. Willett et al., pp. 55–74, Geol. Soc. of Am., Boulder, Colo.

Yarnold, J. C. (1994), Tertiary sedimentary rocks associated with the Harcuvar core complex in Arizona (U.S.A.): Insights intopaleogeographic evolution during displacement along a major detachment fault system, *Sediment. Geol.*, *89*, 43–63.

Zagorchev, I. (1992), Neotectonic development of the Struma (Kraigtid) lineament, southwest Bulgaria and northern Greece, *Geol. Mag.*, *129*, 197–222.

Zagorchev, I. (2007), Late Cenozoic development of the Strouma and Mesta fluviolacustrine systems, SW Bulgaria and northern Greece, *Quat. Sci. Rev.*, *26*(22), 2783–2800, doi:10.1016/j.quascirev.2007.07.017.

Zagorchev, I., and J. Dinkova (1990), Geological map of the People's Republic of Bulgaria, 1:100.000 series Petrich, Razlog, Blagoevgrad, Gotse Delchev and Belitsa sheets. Geological Institute, Bulgarian Academy of Sciences, Sofia.